Journal of Volcanology and Geothermal Research 175 (2008) 289–314

Contents lists available at ScienceDirect

Journal of Volcanology and Geothermal Research

journal homepage: www.elsevier.com/locate/jvolgeores

Characteristics, extent and origin of hydrothermal alteration at Mount Rainier Volcano, Cascades Arc, USA: Implications for debris-flow hazards and mineral deposits

David A. John [a,*], Thomas W. Sisson [b], George N. Breit [c], Robert O. Rye [d], James W. Vallance [e]

[a] U.S. Geological Survey, MS-901, 345 Middlefield Rd., Menlo Park, CA 94025, USA
[b] U.S. Geological Survey, MS-910, 345 Middlefield Rd., Menlo Park, CA 94025, USA
[c] U.S. Geological Survey, MS-964, Federal Center, Denver, CO 80225, USA
[d] U.S. Geological Survey, MS-963, Federal Center, Denver, CO 80225, USA
[e] U.S. Geological Survey, Cascades Volcano Observatory, 1300 SE Cardinal Ct., Suite 100, Vancouver, WA 98683, USA

ARTICLE INFO

Article history:
Received 1 June 2007
Accepted 2 April 2008
Available online 2 June 2008

Keywords:
hydrothermal alteration
volcano hazards
debris flows
O, H, S stable isotopes, magmatic-hydrothermal system

ABSTRACT

Hydrothermal alteration at Mount Rainier waxed and waned over the 500,000-year episodic growth of the edifice. Hydrothermal minerals and their stable-isotope compositions in samples collected from outcrop and as clasts from Holocene debris-flow deposits identify three distinct hypogene argillic/advanced argillic hydrothermal environments: magmatic-hydrothermal, steam-heated, and magmatic steam (fumarolic), with minor superimposed supergene alteration. The 3.8 km^3 Osceola Mudflow (5600 y BP) and coeval phreatomagmatic F tephra contain the highest temperature and most deeply formed hydrothermal minerals. Relatively deeply formed magmatic-hydrothermal alteration minerals and associations in clasts include quartz (residual silica), quartz–alunite, quartz–topaz, quartz–pyrophyllite, quartz–dickite/kaolinite, and quartz–illite (all with pyrite). Clasts of smectite–pyrite and steam-heated opal–alunite–kaolinite are also common in the Osceola Mudflow. In contrast, the Paradise lahar, formed by collapse of the summit or near-summit of the edifice at about the same time, contains only smectite–pyrite and near-surface steam-heated and fumarolic alteration minerals. Younger debris-flow deposits on the west side of the volcano (Round Pass and distal Electron Mudflows) contain only low-temperature smectite–pyrite assemblages, whereas the proximal Electron Mudflow and a <100 y BP rock avalanche on Tahoma Glacier also contain magmatic-hydrothermal alteration minerals that are exposed in the avalanche headwall of Sunset Amphitheater, reflecting progressive incision into deeper near-conduit alteration products that formed at higher temperatures.

The pre-Osceola Mudflow alteration geometry is inferred to have consisted of a narrow feeder zone of intense magmatic-hydrothermal alteration limited to near the conduit of the volcano, which graded outward to more widely distributed, but weak, smectite–pyrite alteration within 1 km of the edifice axis, developed chiefly in porous breccias. The edifice was capped by a steam-heated alteration zone, most of which resulted from condensation of fumarolic vapor and oxidation of H_2S in the unsaturated zone above the water table. Weakly developed smectite–pyrite alteration extended into the west and east flanks of the edifice, spatially associated with dikes that are localized in those sectors; other edifice flanks lack dikes and associated alteration. The Osceola collapse removed most of the altered core and upper east flank of the volcano, but intensely altered rocks remain on the uppermost west flank.

Major conclusions of this study are that: (1) Hydrothermal–mineral assemblages and distributions at Mount Rainier can be understood in the framework of hydrothermal processes and environments developed from studies of ore deposits formed in analogous settings. (2) Frequent eruptions supplied sufficient hot magmatic fluid to alter the upper interior of the volcano hydrothermally, despite the consistently deep (≥8 km) magma reservoir which may have precluded formation of economic mineral deposits within or at shallow depths beneath Mount Rainier. The absence of indicator equilibrium alteration-mineral assemblages in the debris flows that effectively expose the volcano to a depth of 1–1.5 km also suggests a low potential for significant high-sulfidation epithermal or porphyry-type mineral deposits at depth. (3) Despite the long and complex history of the volcano, intensely altered collapse-prone rocks were spatially restricted to near the volcano's conduit system and summit, and short distances onto the upper east and west flanks, due to the necessary supply of reactive components carried by ascending magmatic fluids. (4) Intensely altered rocks were removed from the summit, east flank, and edifice interior by the Osceola collapse, but remain on the upper west flank in the Sunset Amphitheater area and present a continuing collapse hazard. (5) Visually conspicuous rocks on the lower east and mid-to-lower west flanks are not intensely altered and probably have not significantly

* Corresponding author. Tel.: +1 650 329 5424; fax: +1 650 329 5491.
E-mail address: djohn@usgs.gov (D.A. John).

0377-0273/$ – see front matter. Published by Elsevier B.V.
doi:10.1016/j.jvolgeores.2008.04.004

weakened the rock, and thus do not present significant collapse hazards. (6) Alteration developed most intensely within breccia units, because of their high permeability and porosity. Volcanoes with abundant near-conduit upper-edifice breccias are prone to alteration increasing the possibility of collapse, whereas those that are breccia-poor (e.g., massive domes) are less prone to alteration.

Published by Elsevier B.V.

1. Introduction

Mount Rainier towers over the Puget Sound lowland and the Seattle–Tacoma metropolitan area of western Washington (Fig. 1). The last sizeable eruption of this glacier-covered andesitic stratovolcano was ~1000 years-before-present (y BP), but small eruptions may have been as recent as 1894. Besides eruptions, about 55 Holocene lahars have been recognized from Mount Rainier (Crandell, 1971), many of which flowed across regions that are now densely populated. Future lahars could affect 100,000s of people who reside in the Puget Sound lowland (Fig. 2; Scott et al., 1995; Hoblitt et al., 1998; Sisson et al., 2001). Many far-traveled lahars from Mount Rainier formed from newly erupted hot volcanic products traversing, entraining, and melting glacial snow and ice, but some, including the largest, originated by collapse of the hydrothermally-altered upper-edifice flanks (Crandell, 1971; Scott et al., 1995). Lahars originating by collapse of altered edifice flanks are particularly hazardous owing to their high mobility, which is promoted by low rock strengths and high initial pore-water contents, and also because such collapses may take place early in an eruptive period, thus with little warning, or in rare instances without a concurrent eruption.

Hydrothermal alteration has been irregular at Mount Rainier in time, space, and intensity. Parts of the upper edifice are severely weakened and susceptible to collapse and catastrophic debris flows (Crandell, 1971; Frank, 1985; Zimbelman, 1996; Crowley and Zimbelman, 1997; Finn et al., 2001; Reid et al., 2001), but broad areas of the upper mountain consist of either relatively strong, unaltered volcanic rocks, or of incipiently altered rocks that are discolored and contain some hydrothermal minerals, but with little reduction in rock strength. As a result, qualitative assessments of the distribution of altered rocks are of limited use in evaluating edifice stability and hazards.

Exposures of altered rock are small, remote, and of difficult access on upper Mount Rainier. Some Holocene debris-flow deposits, however, contain abundant hydrothermal alteration products, including materials from the edifice interior that are now concealed by young lava flows and by glacial ice. These debris-flow deposits provide a comprehensive sampling of different alteration types at Mount Rainier. Chief among these is the 5600 y BP, 3.8 km^3 Osceola Mudflow that formed when the upper 1+km and northeast flank of Mount Rainier collapsed during small phreatomagmatic eruptions. The Osceola Mudflow traveled down the White River drainage into the Puget Sound lowland more than 100 km from the volcano and inundated >550 km^2 (Fig. 2; Crandell, 1971; Scott et al., 1995; Vallance and Scott, 1997). The collapse was accompanied by deposition of the hydrothermal–mineral-bearing F tephra, and possibly by the Paradise lahar that descended the south slope of the volcano (Vallance and Scott, 1997). Subsequent eruptions have largely filled the Osceola collapse crater, but a weak hydrothermal system now active at Mount Rainier has locally altered 2000–2600 y BP lava flows near the summit (Frank, 1985, 1995; Zimbelman et al., 2000), and travertine-precipitating springs discharge on the lower flanks of the volcano (Frank, 1985).

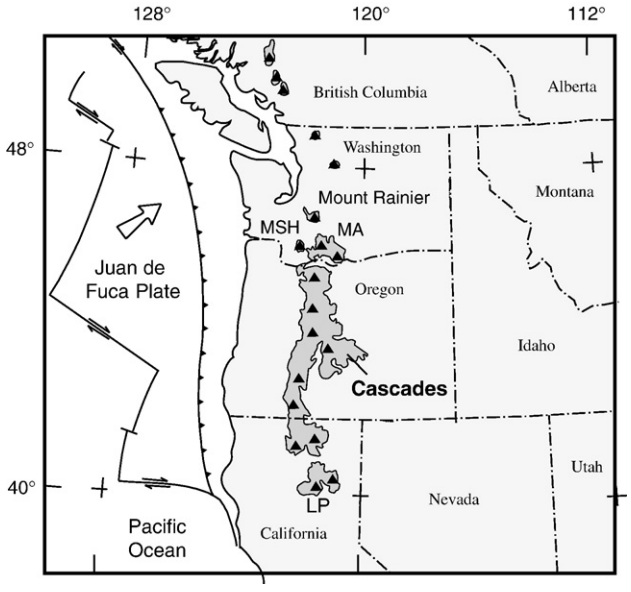

Fig. 1. Index map of western North America showing location of Mount Rainier and Quaternary volcanic rocks of the Cascades. Triangles show Quaternary volcanoes. LP, Lassen Peak; MA, Mt. Adams; MSH, Mt. St. Helens.

In this paper, we characterize hydrothermal alteration of Quaternary rocks at Mount Rainier and reconstruct the distribution of altered rocks at the time of the Osceola Mudflow collapse. Our studies concentrate on Holocene debris flows and tephras that contain fragments of hydrothermally-altered rocks. Characteristics of the debris flows, including their source areas and ages, distribution, range of alteration-mineral assemblages, and the chemical and stable-isotope composition of the hydrothermal minerals, vary around the volcano. By combining our new results with published field (Fiske et al., 1963; Crandell, 1971; Frank, 1985, 1995; Zimbelman, 1996; Bruce, 1998; Zimbelman et al., 2000; Sisson et al., 2001), remote sensing (Crowley and Zimbelman, 1997), and geophysical studies (Moran et al., 2000; Finn et al., 2001), we interpret the probable distribution and origin of hydrothermally-altered rocks on Mount Rainier shortly prior to eruption of the F tephra, edifice collapse, and formation of the Osceola Mudflow at 5600 y BP. Our results and interpretation aid in understanding and predicting edifice-collapse hazards at Mount Rainier by explaining the spatially localized distribution of collapse-prone intensely altered rocks on the upper edifice. This work also helps to account for the large differences in degree of alteration of other Cascades stratovolcanoes by identifying various geologic factors that promote intense hydrothermal alteration within edifice interiors. Our results also are relevant to understanding why hydrothermal systems in some stratovolcanoes are associated with formation of porphyry and related epithermal mineral deposits, whereas other systems are not.

2. Tectonic and geologic setting of Mount Rainier

Mount Rainier, Mount St Helens and Mount Adams are active stratovolcanoes of the Cascades arc in southern Washington State that result from east-northeasterly subduction of the oceanic Juan de Fuca plate beneath North America (Fig. 1). The Cascades arc is under compression from Mount Rainier northward (Wells et al., 1998) leading to strong basement uplift. A primary result of this compression for Mount Rainier is that magma flux is strongly localized to the volcano's axial conduit system and associated radial dikes, with almost no diffuse peripheral volcanism.

Mount Rainier overlies a thick accumulation of Oligocene and Miocene arc volcanic rocks of the Ohanapecosh, Stevens Ridge, and Fife's Peak Formations and intrusive granodiorite of the middle to late

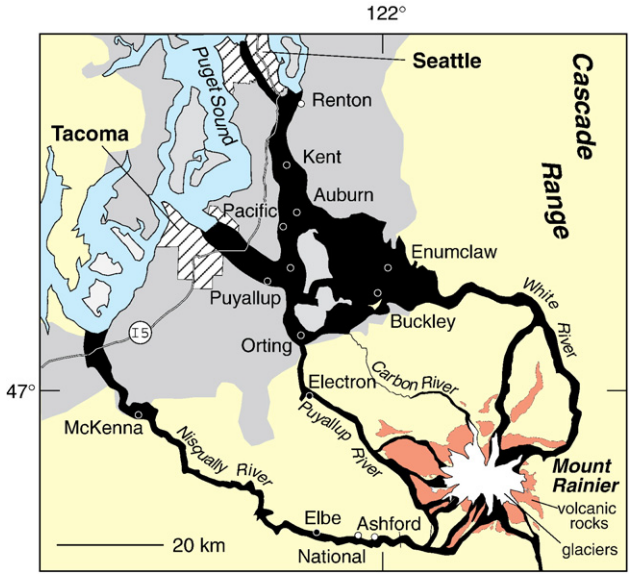

Fig. 2. Map showing Holocene lahars and their paths into Puget Sound lowland. Modified from Sisson et al. (2001).

Miocene Tatoosh Pluton (Fiske et al., 1963; Mattinson, 1977; Vance et al., 1987). The Tertiary substrate crops out as high as ~2200 m above sea level (asl) in valleys and ridges surrounding Mount Rainier's flanks, showing that the volcano sits atop a basement topographic high that was uplifted and exhumed in the last ~10 my (Walsh et al., 1987; Reiners et al., 2002).

3. Summary of Quaternary Mount Rainier stratovolcano

Mount Rainier mostly comprises andesite to low-SiO_2 dacite lava flows and fragmental deposits (breccias, pyroclastic flows), subordinate tephras, and a single preserved lava dome. Headwalls and ridges on the upper volcano (within 5 km of the summit) expose repetitive alternations of cliff-forming dense lava flow interiors and ledge-forming unconsolidated rubbly flow-top breccias, each on the order of 10–30 m thickness and dipping 15–30° radially away from the summit. Lava flows on the lower edifice flanks (up to 20 km from the summit) are much thicker, in places reaching 300 m, due to impoundment against Pleistocene valley-filling glaciers (Lescinsky and Sisson, 1998). Typical andesitic eruptive products are rich (to 40%) in phenocrysts of plagioclase, hypersthene, augite, titanomagnetite, and ilmenite, and contain accessory apatite, and traces of pyrrhotite almost exclusively as blebs encased in phenocrysts. Minor amphibole phenocrysts are present in some andesites and in many dacites; olivine is common in basaltic andesites.

The modern Mount Rainier edifice started to grow about 500,000 y BP, atop the deeply eroded remains of an ancestral Mount Rainier volcano that was active from ~2–1 Ma (Sisson and Lanphere, 1997). Volcanic activity continued intermittently between the ancestral and modern edifices, as shown by isolated, deeply incised lava flows of intermediate age exposed in the upper reaches of some valleys with

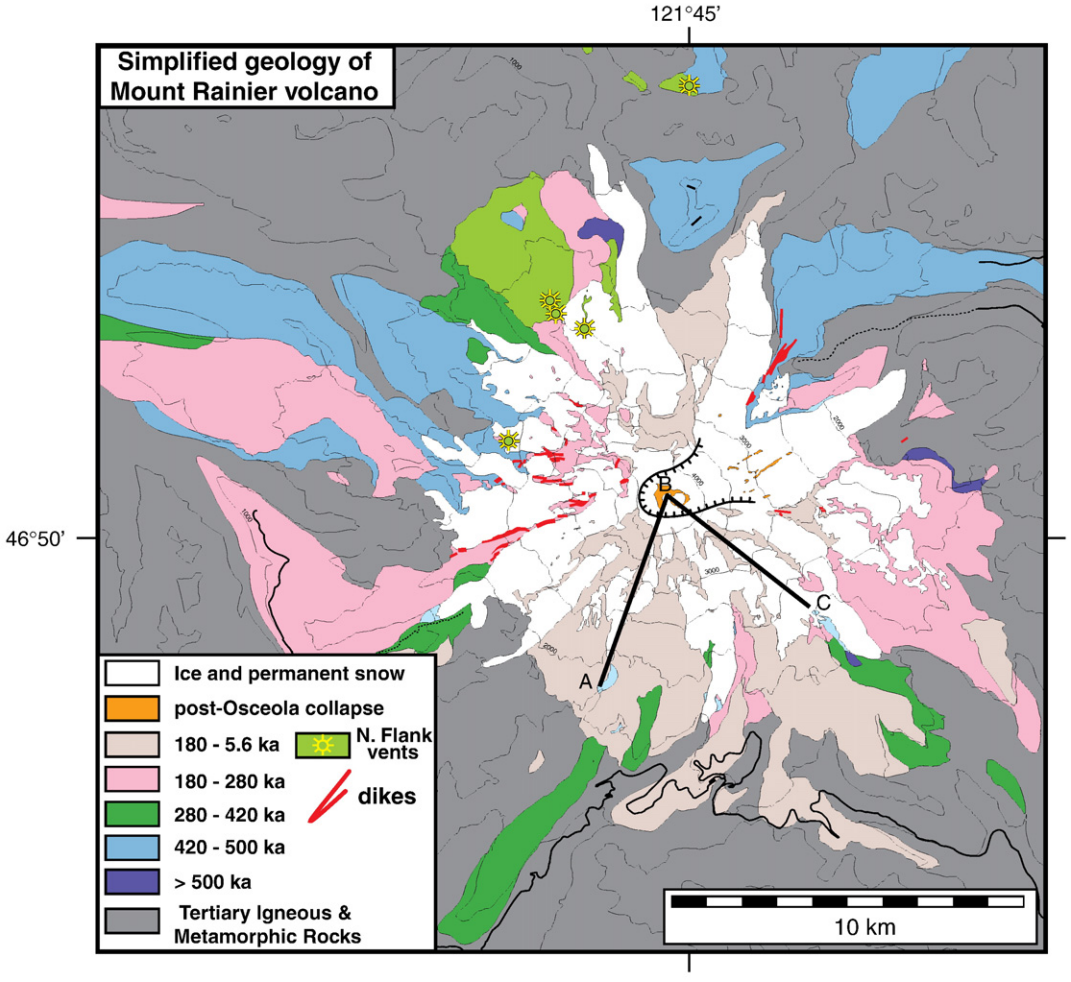

Fig. 3. Generalized geologic map of Mount Rainier showing major stages of edifice construction. Black lines and points A, B, and C outline cutaway view shown in Fig. 11.

heads terminating on the volcano. Since 500,000 y BP, however, frequent eruptions have produced a voluminous and nearly continuous rock record that constitutes the bulk of the Mount Rainier edifice (Fig. 3). Effusion rates varied substantially during growth of the modern edifice (Sisson et al., 2001), with periods of high effusion of 80,000 and 100,000 years duration (500,000 to 420,000 y BP and 280,000 to 180,000 y BP), leading to rapid edifice growth and widespread voluminous flank lava flows, separated by periods of modest effusion of 140,000 and 180,000 years, the latter leading to stasis or edifice degradation. Effusion rates also varied within the growth stages, with most of the lava flows of the upper north and south flanks of the edifice having erupted at 20,000 to 40,000 y BP, and with many unconformities and disconformities between lava flow sequences recording hiatuses too brief (<10,000 years) to resolve by current dating methods.

East-northeast-striking radial dikes with nearly vertical dips (Fig. 3) were intruded mainly during the two periods of high effusion from 500,000 to 420,000 y BP and from 280,000 to 180,000 y BP, but a few younger dikes are also present (Sisson et al., 2001). Localization of dikes on the west and east flanks of the edifice may result from exploitation of preexisting weaknesses in the shallow basement, such as common east-northeast-striking joints that are perpendicular to broad north-northwest trending folds in Tertiary strata. Most dikes are 2–5 m thick and are exposed as far as ~7 km from the summit. Some dikes fed flank lava flows, as demonstrated by dikes that can be traced into lava flows on the west flank of the volcano and by a large dike at St. Elmo Pass and the nearby voluminous andesite of Burroughs Mountain on the volcano's lower east flank (Stockstill et al., 2002). Radial dikes on the lower flanks end near the beginning of exposed Tertiary basement, consistent with lateral propagation of the dikes from the axial conduit system at edifice levels.

A significant event in Mount Rainier's history was the major edifice flank collapse of 5600 y BP that removed the volcano's summit and upper east flank, producing the 3.8 km^3, alteration-mineral-rich Osceola Mudflow (Crandell and Waldron, 1956; Vallance and Scott, 1997). The collapse left an amphitheater-shaped crater ~1.5 km across, open to the northeast. The back wall and rim of this crater are preserved as small peaks and rock knobs that partly encircle the present summit to the north, northwest, southwest, and southeast (Figs. 3 and 4). The collapse removed dikes and altered rock from the upper ~1500 m of the volcano's east flank and summit area. Subsequent lava eruptions largely filled the collapse crater, building a new summit cone capped by a pair of partly overlapping 400-m-diameter craters. Rocks of the new summit cone are almost everywhere concealed by thick glaciers, but windows through the ice at 3000–3600 m elevation expose glassy, non-altered lava flows, similar to unaltered lava flows that form the east half of the east summit crater. All exposures of the west summit, as well as the western half of the younger east summit crater, are hydrothermally altered (Fig. 4; Frank 1995; Zimbelman 1996; Zimbelman et al., 2000), although geophysical measurements (Finn et al., 2001) indicate that this summit alteration is thin (<20–50 m) and that most of the post-Osceola summit cone consists of unaltered volcanic rocks.

4. Depths of Mount Rainier magmas and their intensive conditions

Andesite–dacite magmas of Mount Rainier are calc-alkaline (McKenna, 1994; Venezky and Rutherford, 1997; Stockstill et al., 2002), relatively oxidized, moderately hydrous, and ascend through a complex plumbing system that probably lacks a large long-lived near-surface (≤8 km) magma reservoir. Coexisting Fe–Ti-oxide rim compositions indicate pre-eruptive temperatures of ~850–1025 °C and oxygen fugacities typically 1–2 log units more oxidized than the Ni–NiO buffer, although a few samples are as reduced as Ni–NiO (Venezky and Rutherford, 1997; Kirn, 1995; T. Sisson unpublished analyses). Melt inclusions in tephra phenocrysts have dissolved H_2O concentrations of

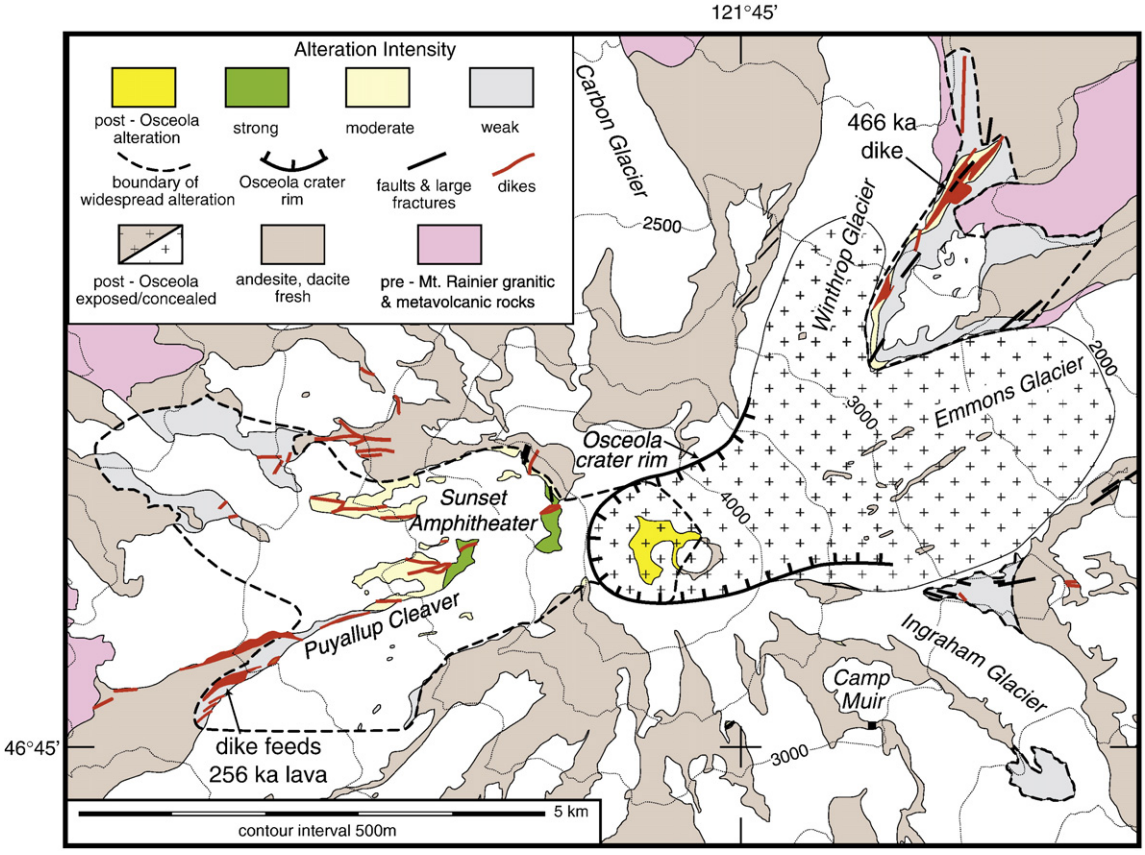

Fig. 4. Map showing surface distribution and intensity of hydrothermally-altered rocks on Mount Rainier. Modified from Sisson et al. (2001).

3–4 wt.% and dissolved CO_2 concentrations from <20 to 900 ppm (T. Sisson unpublished analyses), consistent with pre-eruptive storage pressures from 100 to 280 MPa, equivalent to depths of ~4–10 km (assuming average upper crustal density of 2700 kg/m^3). Because of the potential for leakage of volatiles from melt inclusions, and for partitioning of CO_2 into shrinkage bubbles, the greater depths are more reliable estimates of magma stagnation levels. Absence of a large near-surface magma reservoir is also consistent with the restriction of surface thermal features to within 2 km radially from the summit (Frank, 1985), a lack of distributed volcanic vents for the modern and ancestral edifices, and with concentrated brittle failure-type seismicity centered beneath the edifice at upper crustal depths (Moran et al., 2000). Seismic velocities consistent with elevated temperatures and the potential presence of magma do not commence until depths >8 km beneath the edifice base (Moran et al., 1999).

5. Summary of Holocene debris flows

Holocene lahars from Mount Rainier have one of three origins: (1) collapse of hydrothermally-altered parts of the edifice; (2) interaction of hot rock with ice during eruptions; and (3) mixing of clastic debris and water caused by glacial outburst floods, failure of water-saturated debris, or heavy rainfall.

Several large- to very-large-volume lahars at Mount Rainier were initiated by collapse of hydrothermally-altered regions of the upper edifice (Crandell, 1971; Scott et al., 1995; Vallance and Scott, 1997). The altered rocks and the resulting lahars contain abundant hydrothermally formed clay minerals. The avalanches of altered rock transformed to lahars as they flowed rather than continuing to slide as debris avalanches, because the altered rock was weak and because clay-rich domains held large amounts of pore water within the disaggregating rock debris (Vallance and Scott, 1997). Numerous large lahars also formed at Mount Rainier by the eruption of hot rock or magma onto snow and ice, such as during pyroclastic flows. Small lahars are generated nearly every year at Mount Rainier when heavy rains fall, when glaciers suddenly release water, or when streams are diverted or captured. These small lahars are also clay poor, but are not related to eruptions at the volcano. Clay-poor lahars, whether eruption related or generic, have no relation to hydrothermal alteration at the volcano.

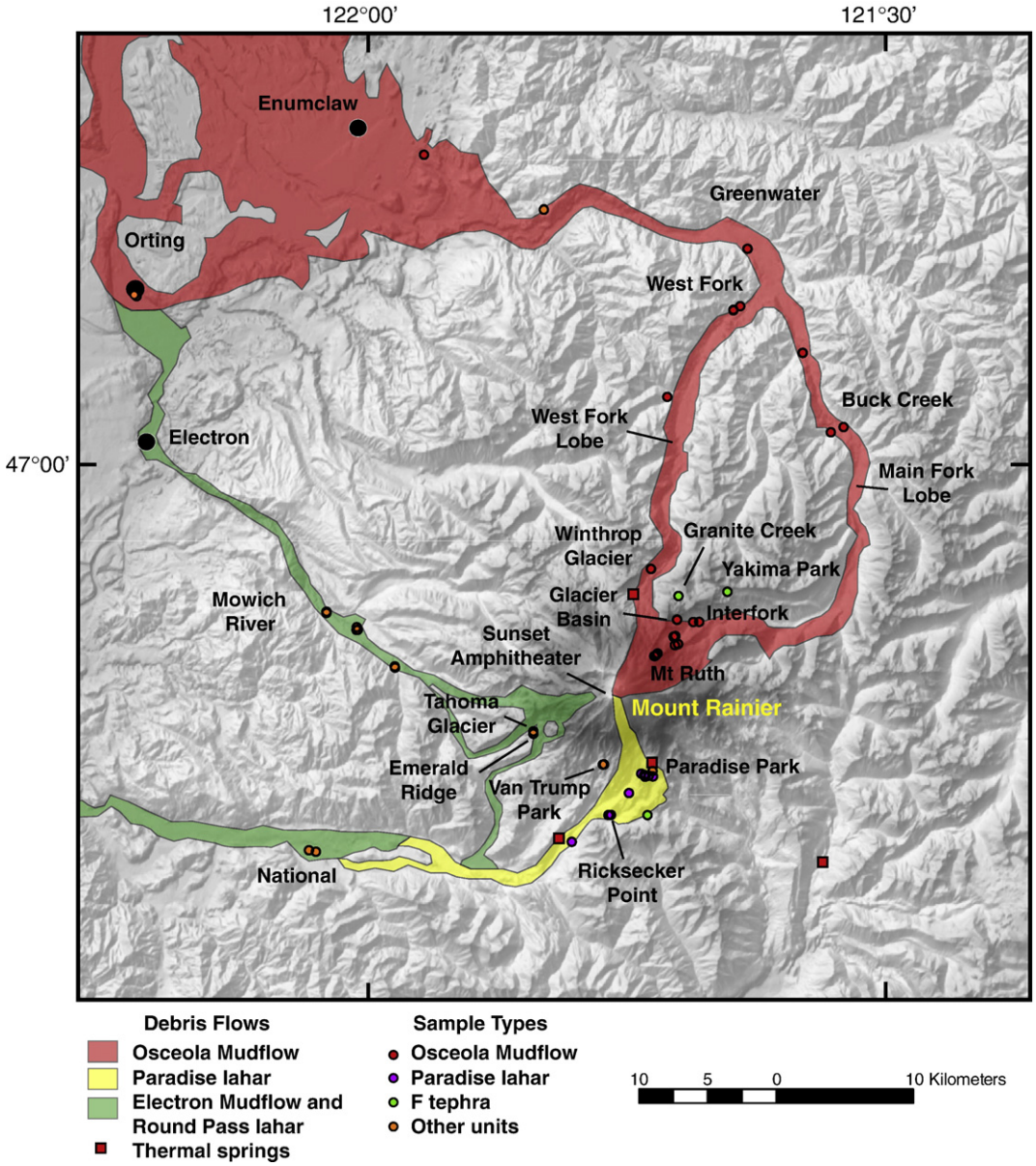

Fig. 5. Shaded relief map showing the distribution of Holocene clay-rich lahars, sample locations, names, and thermal springs on the lower flanks of Mount Rainier.

Of seven edifice- or flank-collapse-induced and clay-rich Holocene lahars, six were during eruptive periods and one was at a time for which no eruption is documented. Clay-rich lahars range in age from about 10,000 to 500 years old and in volume from about 5×10^7 to 4×10^9 m^3. Edifice collapses of hydrothermally-altered rock and the clay-rich lahars they generated were confined to the south flank of Mount Rainier before 5600 y BP, to the west flank after 5600 y BP, but affected the northeast flank during the eruption of about 5600 y BP. A summary of clay-rich lahars, their ages, direction, and relation to eruptions is as follows (Crandell, 1971; and J. Vallance, unpublished):

Van Trump debris flow	9500–10,000 y BP	South	During an eruptive period
Reflection Lakes lahar	6800–7200 y BP	South	During an eruptive period
Paradise debris flow	5600–6000 y BP	South	During an eruptive period
Osceola Mudflow	5600 y BP	NE	Coeval with tephra layer F
Round Pass mudflow	2600–2700 y BP	West	During an eruptive period
Unnamed	1000–1100 y BP	West	During an eruptive period
Electron Mudflow	500 y BP	West	No known eruption

The Osceola Mudflow descended the northeastern slopes of the volcano, filled valleys of the White River to depths of 80–150 m, spread over more than 200 km^2 of Puget Sound lowland and flowed under water of Puget Sound to near the present sites of the ports of Tacoma and Seattle (Figs. 2 and 5; Vallance and Scott, 1997). Vallance and Scott suggested that the Osceola edifice collapse may have developed as several successive slide blocks, the first of which included the outer less-altered carapace of the volcano and the last of which included the deepest and most intensely altered core of the edifice. Downstream, the components of the initial slide block were deposited first along valley margins or at depth, whereas deposits of the last slide block were deposited along axial parts of valleys and across distal areas of Puget Sound lowland. Axial deposits commonly contain numerous hydrothermal minerals and huge volumes of hydrothermal clay (as much as 17% by total weight). The coeval F tephra consists of a pumiceous layer distributed broadly to the east of the volcano sandwiched between fine-grained tephra layers rich in hydrothermal minerals identical to those in the Osceola Mudflow. The clay-rich members of the F tephra were deposited to the northeast of the volcano along an axis that coincides with the outlet direction of the Osceola collapse scar. This distribution, along with other geologic observations (Vallance and Scott, 1997), is evidence that the hydrothermal–mineral-rich members of the F tephra resulted from northeasterly directed explosive expansion of the interior hydrothermal system of the active edifice during failure and decompressive unloading.

6. Hydrothermal systems and alteration at Mount Rainier

Mount Rainier contains altered rocks currently forming from the active hydrothermal system, as well as more widespread altered rocks that formed earlier when hydrothermal processes were more vigorous and extensive than at present. Hydrothermal activity probably never died out completely since inception of the present edifice, but expanded and contracted with the overall magmatic flux. This waxing and waning behavior is demonstrated in field exposures of strongly altered rocks overlain unconformably by unaltered rocks that pass along strike into altered rocks. Although our attempts to date hydrothermal minerals using $^{40}Ar/^{39}Ar$ methods have been unsuccessful, it is likely that many or most of the rocks contained in Holocene debris-flow deposits were altered well before the collapse event that spawned the particular debris flow. Our study focuses on this long-term hydrothermal history of the volcano that controls edifice flank instability. Previous studies of the small, currently active hydrothermal system are summarized below.

6.1. Mount Rainier's active hydrothermal system

A weak, active hydrothermal system at Mount Rainier has locally altered post-5600 y BP lava flows that infill the Osceola Mudflow collapse crater (Figs. 3 and 4; Frank, 1985, 1995; Zimbelman et al., 2000; Sisson et al., 2001). Frank mapped heated ground, fumaroles, and hydrothermally-altered rocks that cover an area of about 12,000 m^2 at the East and West Craters on the volcano's summit. Fumarole temperatures reach 82 °C, the approximate boiling temperature for water at the summit elevation, and alteration phases include smectite, halloysite, kaolinite, silica phases (cristobalite, tridymite, opal), alunite, gibbsite, and calcite. Zimbelman et al. (2000) studied fumarole gases and condensates in ice caves near the summit and noted the presence of sulfate minerals encrusting a fumarole vent indicating locally high H_2S or SO_2 contents in past fumaroles. Measured temperatures of two fumaroles at the summit were 62 °C in 1997.

Frank (1985, 1995) and Symonds et al. (2003a,b) described thermal springs on the lower flanks and around the base of Mount Rainier. Thermal springs discharging from the Quaternary andesites are low temperature, neutral pH, SO_4-enriched solutions that may be derived from the outflow of acid sulfate–chloride solutions from the axial hydrothermal system diluted by shallow cold meteoric water. Thermal springs in Tertiary basement rocks at lower elevations beyond the base of the present volcano are Cl-enriched, have a neutral pH, and locally precipitate travertine. Parent fluids for these springs possibly originate in the deeper parts of Mount Rainier's hydrothermal system at depths below the boiling zone and contain a large component of CO_2 and CH_4 derived from shallow crustal sources.

6.2. Fossil hydrothermal systems at Mount Rainier

6.2.1. Alteration mineralogy and mineral associations

Alteration minerals were identified in about 325 samples of Quaternary material from Mount Rainer (Fig. 5 and Supplementary data; analytical methods are described in Appendix A). Samples included (1) altered rocks cropping out on the volcano, (2) bulk matrix samples of Holocene debris flows, (3) clasts within Holocene debris flows, and (4) tephras. Debris-flow deposits sampled were the Osceola, Round Pass, and Electron Mudflows, the Van Trump, Reflection Lake, Paradise, and National lahars, and the Tahoma Glacier rockfall.

Common groups of alteration minerals on Mount Rainier define nine major hypogene associations formed by hydrothermal processes and one supergene assemblage formed by surficial weathering (Table 1). We use the term "alteration association" for common groupings of minerals independent of thermodynamic equilibrium constraints. As noted in the association descriptions below, there is considerable overlap and variation in mineralogy among these associations, reflecting variable conditions of alteration during waxing and waning of hydrothermal activity and superimposed episodes of alteration. Major types of alteration described below generally follow the nomenclature of Meyer and Hemley (1967).

6.2.1.1. Smectite–pyrite. Intermediate argillic smectite–pyrite alteration is the most abundant alteration association. Smectite–pyrite altered rocks are common in all Holocene clay-rich debris flows and comprise most of the weak to moderate intensity alteration exposed at the surface (Fig. 4). The intensity of smectite–pyrite alteration varies from very weak to nearly complete. Completely altered rocks consist of pervasive replacement of all primary minerals and glass by smectite and pyrite, whereas weakly altered rocks consist of partial replacement of glass and mafic phenocrysts (mostly pyroxene) by smectite, pyrite and silica phases, and pyrite replacement of magnetite (Fig. 6A). Narrow (typically <1 mm wide) pyrite veins, with patches of anhydrite partly to completely replaced by gypsum, and minor barite are common in this association (Fig. 6B). Vesicles partly filled with pyrite, smectite, silica phases, and/or anhydrite/gypsum are common in weakly altered rock in this association. X-ray diffraction (XRD) and SEM-EDS analyses of smectite are consistent with classification as montmorillonite, but local variations in iron, magnesium and aluminum content suggest a range in

Table 1
Characteristics of hydrothermal alteration at Mount Rainier

	Alteration association								
	1	2	3	4	5	6	7	8	9
Assemblage name	Smectite–pyrite	Illite/smectite–chlorite–pyrite	Opal–kaolinite	Jarosite–alunite–opal	Kaolinite–opal–pyrite	Quartz–pyrophyllite–pyrite	Quartz–illite–pyrite	Quartz–topaz–pyrite	Quartz–pyrite
Phenocryst alteration									
Plagioclase	Smectite	Illite or mixed-layer I/S	Opal, kaolinite, alunite	Opal, local kaolinite, alunite	Opal, local alunite or dickite	Silica phases or alunite	Illite	Topaz, quartz	Leached
Mafic minerals	Smectite, pyrite	Chlorite, I/S, pyrite	Opal	Opal	Opal, kaolinite, alunite, pyrite	Silica phases	Illite	Topaz, quartz, pyrite	Leached
Oxides	Pyrite, TiO_2 phase; relict ilmenite in weak alteration	Pyrite	Fe-oxides, TiO_2	Fe-oxides, TiO_2	Pyrite, TiO_2	Pyrite	Pyrite	Pyrite, TiO_2	Pyrite
Groundmass alteration	Smectite, pyrite, gypsum/anhydrite	Illite/smectite, pyrite, silica phases	Opal, kaolinite, alunite	Opal, alunite, jarosite	Silica phases, kaolinite, alunite, pyrite, gypsum/anhydrite	Silica phases, pyrite, alunite, pyrophyllite, gypsum/anhydrite	Quartz, illite, pyrite	Quartz, topaz, pyrite	Quartz, pyrite
Silica phases	Quartz, opal-A/CT, opal-C, cristobalite	Quartz, opal C/cristobalite	Opal-A/CT	No data (opal phase(s))	Opal-CT, local quartz	Quartz, opal-CT	Quartz, tridymite	Quartz, cristobalite	Quartz
Open-space filling	Pyrite, chalcedony, smectite, gypsum/anhydrite	Quartz, pyrite, gypsum/anhydrite	Alunite, kaolinite, anhydrite/gypsum, sulfur	Alunite, jarosite, sulfur	Pyrite, silica phases, alunite, kaolinite, gypsum/anhydrite	Alunite, pyrophyllite, pyrite	Not observed	Not observed	Pyrite, gypsum
Veins	Narrow pyrite, gypsum, smectite	Not observed	Not observed	Not observed	Very narrow pyrite, opal, gypsum	Very narrow pyrite, gypsum	Not observed	Not observed	Not observed
Other minerals	Local trace kaolinite, illite, pyrophyllite, barite	–	Local trace pyrite	–	Local trace sulfur, fluorite	Local trace enargite	Local trace pyrophyllite	Anhydrite/gypsum, trace sulfur	Trace alunite, pyrophyllite, illite
Alteration intensity	Very weak to strong	Generally strong	Generally strong	Generally strong	Very strong	Very strong	Very strong	Very strong	Very strong
Texture	Dense except vesicular rocks	Dense	Porous, very fine grained	Porous, brecciated	Dense to porous, brecciated	Dense, brecciated	Dense to porous, brecciated	Porous	Porous
Alteration controls	Primary permeability (igneous breccias); fracture zones; margins of dikes; vesicules; perched aquifers	Primary permeability (igneous breccias)	Primary permeability (igneous breccias); acid-leaching	Primary permeability (igneous breccias)	Primary permeability (igneous breccias); hydrothermal brecciation	Primary permeability (igneous breccias); hydrothermal brecciation	Primary permeability (igneous breccias); acid-leaching	Acid-leaching	Acid-leaching
Temperature of formation (°C)	<100–175	175–250	<100–125	<100–150	150–225	225–300; 150–200(?) in Van Trump and Paradise lahars	225–300	200–300	200–300
Hydrothermal environment of formation (Rye, 2005)	Magmatic-hydrothermal, fringe of steam-heated	Magmatic-hydrothermal	Steam-heated	Magmatic steam	Magmatic-hydrothermal	Magmatic-hydrothermal	Magmatic-hydrothermal	Magmatic-hydrothermal	Magmatic-hydrothermal

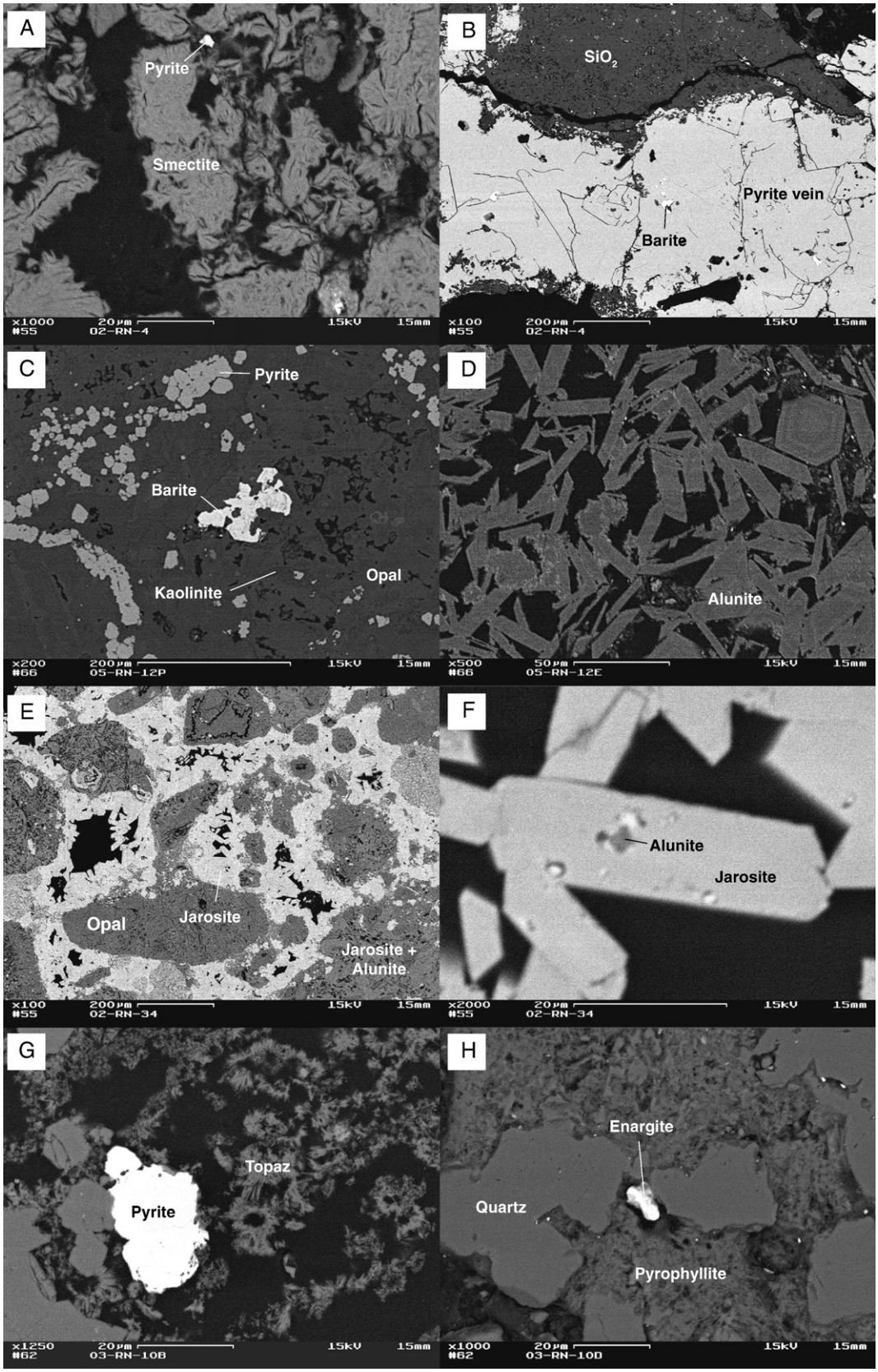

Fig. 6. Back-scattered SEM images showing hydrothermal alteration features. (A) Typical fine-grained smectite–pyrite alteration of andesite clast in Tahoma Glacier rockfall. (B) Smectite–pyrite alteration with coarse-grained pyrite and barite filling narrow (<1 mm) vein. Clast in Tahoma Glacier rockfall. (C) Opal–kaolinite–pyrite alteration with barite. Clast in Osceola Mudflow. (D) Relatively coarse-grained zoned alunite crystals in clast in Osceola Mudflow. Brighter areas are enriched in K. (E) Opalized breccia cemented with coarse crystalline jarosite and mixtures of jarosite and alunite. Clast in Paradise lahar. (F) Enlargement of (E) showing euhedral jarosite with alunite inclusion. (G) Quartz–topaz–pyrite altered clast in Osceola Mudflow. (H) Quartz–pyrophyllite–pyrite alteration with small enargite (Cu_3AsS_4) crystal. Clast in Osceola Mudflow.

composition. XRD analyses of <2 μm separates detected the presence of minor kaolinite ± pyrophyllite in some samples of intense smectite–pyrite alteration, likely resulting from cross-cutting higher grade alteration (as indicated by the presence of pyrophyllite, which typically forms at higher temperature except in the presence of amorphous silica; Reyes, 1990).

6.2.1.2. Illite–chlorite–pyrite. Several intensely altered clasts in the West Fork lobe of the Osceola Mudflow contain mixed-layer illite–smectite or well-crystallized illite, chlorite, quartz or cristobalite, and abundant disseminated pyrite.

6.2.1.3. Opal–kaolinite ± alunite ± sulfur. This advanced argillic alteration association is relatively common in clasts in the Osceola Mudflow, Paradise lahar, and Tahoma Glacier rockfall. It also is present in clasts in the Van Trump lahar and in rock exposed near the summit, especially at West Crater (Frank, 1985). Most debris-flow clasts with this association are intensely altered breccias comprised of fine to very fine-grained (<2 μm) kaolinite, alunite, and opal (dominantly opal-A and opal-CT), with minor Ti-oxide and/or Fe-oxide phase(s) (hematite, goethite). Pyrite generally is absent. Trace amounts of smectite were detected by XRD in some samples. Elemental sulfur locally fills vugs, and barite and anhydrite/gypsum are present locally in trace amounts. Alunite commonly forms very fine-grained pseudocubic crystals. X-ray diffraction and SEM-EDS analyses indicate that most alunite is Na-rich, although complex Na–K zoning is present.

6.2.1.4. Jarosite–alunite–opal. Sparse clasts of brecciated andesite in the Paradise lahar and in the Osceola Mudflow are cemented with fine-grained crystalline jarosite, fine-grained alunite, and opal (Fig. 6E,F). Jarosite typically overgrows and contains inclusions of alunite. Alteration of rock fragments in the breccia varies from complete replacement by opal, replacement of plagioclase phenocrysts with kaolinite or alunite, to partial replacement of groundmass by opal with relict unaltered plagioclase phenocrysts. Anhydrite/gypsum crystals locally fill vesicles lined with alunite. A very fine-grained red Fe-oxide (hematite?) is present locally in the breccia matrix.

6.2.1.5. Kaolinite–opal/tridymite–pyrite ± alunite. This advanced argillic alteration association has been found only in breccia clasts in the Osceola Mudflow, primarily in the Main Fork lobe, and in Tahoma Glacier rockfall. Rocks in this association contain up to 25 vol.% fine-grained pyrite and local marcasite that forms disseminated crystals and breccia matrix and fills narrow veins (Fig. 6C). Fine-grained silica phases (opal-A, opal-CT, or tridymite), kaolinite, and alunite replace breccia fragments. Fine-grained pyrite, silica phases, alunite, and/or kaolinite form the breccia matrix. Alunite generally occurs as fine acicular to tabular crystals up to 50 μm long (Fig. 6D). Alunite crystals tend to be Na-rich, but many have complex Na–K zoning and locally have P- and Ca-rich zones. Anhydrite/gypsum is present both as poikilitic crystals in breccia matrix and in narrow veins. Trace amounts of barite, fluorite, and elemental sulfur are present in some clasts. Dickite–quartz and/or opal-CT–pyrite–minor alunite is an uncommon variant of this association in several thoroughly altered clasts in the Osceola Mudflow. Dickite replaces plagioclase phenocrysts, and a porous mixture of quartz or opal-CT and pyrite replaces the groundmass in these clasts.

6.2.1.6. Quartz or opal-CT–pyrophyllite–anhydrite–pyrite ± kaolinite ± alunite. This relatively uncommon advanced argillic association was found only in pervasively altered breccia clasts in the Osceola Mudflow and as single clasts from the Van Trump and Paradise lahars. Fine-grained quartz and/or opal-CT, pyrite, and local alunite replace breccia fragments. Fine-grained silica phases, pyrophyllite, pyrite, and anhydrite/gypsum, with local kaolinite and/or alunite, form the breccia matrix. Narrow veinlets of anhydrite/gypsum and pyrite are common. Trace amounts of enargite are present in the matrix of one breccia sample from the Osceola Mudflow (Fig. 6H). Multiple stages of hydrothermal alteration and brecciation are evident in some samples (Fig. 7H).

6.2.1.7. Quartz–illite–pyrophyllite–pyrite. This uncommon advanced argillic alteration association was found only in clasts in the Osceola Mudflow. It consists mostly of fine-grained quartz and/or tridymite and pyrite with minor to trace amounts of very fine-grained illite and pyrophyllite.

6.2.1.8. Quartz–topaz–anhydrite–pyrite. This uncommon advanced argillic alteration association was found only in clasts in the Osceola Mudflow. Alteration is texturally destructive, leaving a porous intergrowth of fine-grained quartz and/or cristobalite, topaz, and pyrite (Fig. 6G). Anhydrite/gypsum is present in the groundmass of one sample.

6.2.1.9. Quartz–pyrite (residual silica). This alteration was found only in clasts in the Osceola Mudflow. Alteration is texturally destructive and leaves a porous residue of fine-grained quartz and pyrite with trace amounts of alunite, pyrophyllite, and/or illite.

6.2.1.10. Supergene alteration. Parts of the debris flows and outcrops within tens of centimeters of the ground surface are modified variably by supergene oxidation of pyrite. Products of this oxidation include orange to black ferric oxyhydroxides, earthy coatings of jarosite, water-soluble iron sulfates, and gypsum. These phases penetrate altered rock clasts as well as the matrices of all clay-rich debris flows and the F tephra. SEM-EDS and isotope analyses determined that alunite and clay minerals are not products of supergene conditions. Water-saturated exposures of the clay-rich debris flows lack these oxidation products and likely retain their depositional composition.

6.2.2. Hydrothermal environments

Hypogene hydrothermal alteration associations and stable-isotope compositions at Mount Rainier define three hydrothermal environments recognized in active and fossil hydrothermal systems elsewhere (e.g., Schoen et al., 1974; Henley and Ellis, 1983; Reyes, 1990; Rye et al., 1992; Giggenbach, 1997; Hedenquist et al., 2000; Rye, 2005). These environments are magmatic-hydrothermal, steam-heated, and magmatic steam (Rye et al., 1992).

The magmatic-hydrothermal environment forms above degassing magmas where supercritical or two phase fluids exsolve that typically evolve at shallower depths to low density vapor and saline brine phases which become separated by buoyancy and viscosity contrasts. The magmatic vapor rich in SO_2, HCl, H_2S, and HF condenses, usually into ground water, at ~350–400 °C, and the SO_2 disproportionates, forming H_2SO_4 and H_2S ($4\ SO_2 + 4\ H_2O = 3\ H_2SO_4 + H_2S$). Hydrolysis reactions of the resulting acid fluid with wall rocks progressively neutralize the acidity while forming hydrothermal minerals that may include pyrophyllite, topaz, dickite, alunite, kaolinite, illite, quartz, anhydrite, and pyrite; montmorillonite may form at lower temperatures and at near-neutral pH. Dissolved gases (mainly H_2S and CO_2) may separate into the H_2O-rich vapor phase upon boiling, and ascend to the surface. The *steam-heated environment* forms where the H_2S is oxidized by atmospheric O_2, within the vadose zone, forming H_2SO_4 ($H_2S + 2O_2 = H_2SO_4$) which is absorbed into steam-heated ground water (Schoen et al., 1974). These steam-heated waters are close to 100 °C and have pH >2. The steam-heated waters alter wall rocks to an advanced argillic assemblage of opal (cristobalite), alunite, kaolinite, and minor pyrite (Schoen et al., 1974). The *magmatic steam environment* differs from the steam-heated environment in that elevated temperature magmatic gases vent directly to the atmosphere without condensing into ground water. In the magmatic steam environment, SO_2-dominant gas rises rapidly to the surface commonly resulting in monomineralic veins of alunite without significant pyrite or wall rock alteration (Rye, 2005) before venting to the atmosphere.

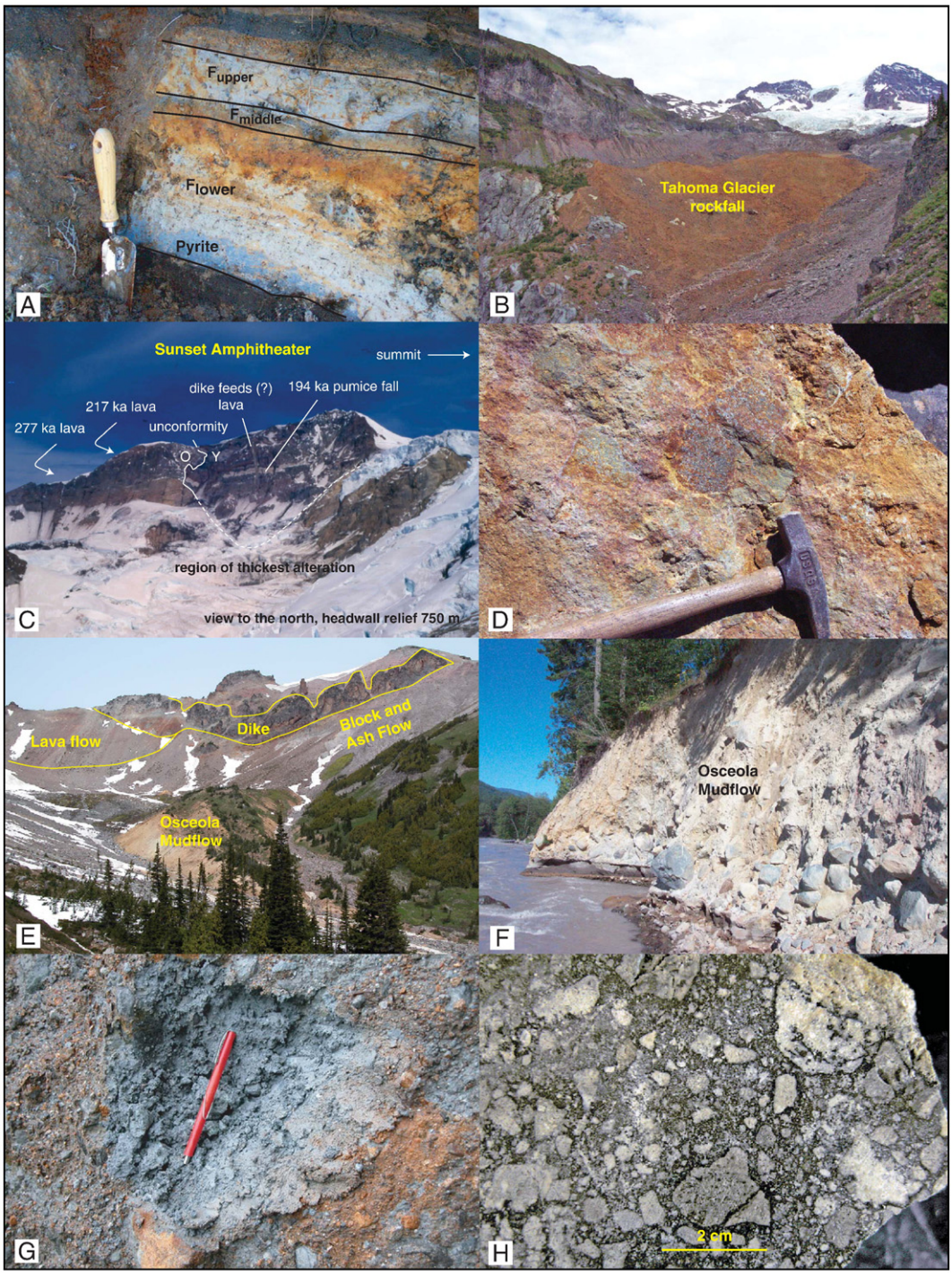

Fig. 7. Photographs showing hydrothermal alteration features. (A) F tephra exposed near head of Granite Creek. F_{upper} and F_{lower} contain abundant hydrothermal minerals including gray pyrite layer, whereas F_{middle} is mostly juvenile materials. (B) View of early 20th Century Tahoma Glacier rockfall (orange rocks) sitting on the toe of Tahoma Glacier. Sunset Amphitheater in background. (C) View of upper Tahoma Glacier and Sunset Amphitheater showing unconformity between strongly altered ~275 ka andesite breccias overlain by unaltered 195 ka white tuff filling channel cut in altered rocks. (D) Typical pyrite-rich smectite–pyrite altered clast in the Tahoma Glacier rockfall. (E) View of Glacier Basin showing 466 ka dike complex intruding ~470 ka block and ash flows. Generally weak, although strongly colored, smectite–pyrite alteration is developed mostly in the wall rocks of the dike. Osceola Mudflow exposed in the bottom of the basin. (F) 8-meter-thick exposure of the Osceola Mudflow in the banks of the White River near Greenwater about 50 km downvalley from Mount Rainier. Note characteristic yellowish color of oxidized Osceola. (G) Close-up of gray pyrite-rich matrix of Osceola Mudflow in upper West Fork of the White River near toe of Winthrop Glacier. Water-saturated exposures of the Osceola are characteristically dark gray and contain up to 5–10% fine-grained pyrite. (H) Hydrothermal breccia clast in the Osceola Mudflow. Clast consists of opal-CT–alunite–pyrophyllite–pyrite–anhydrite/gypsum alteration in matrix of pyrite and silica. Note fractured clast cut by pyrite-rich vein/hydrothermal matrix just above scale bar.

6.2.3. Textures and physical controls on alteration

Hydrothermal activity on Mount Rainier produced several distinct textures including hydrothermal breccias, veins, skeletal residue from acid-leaching, and vesicle-filling minerals. Multiple textural styles commonly are evident within single outcrops or clasts. The textural variations reflect both primary and secondary controls on the movement of altering fluids (Table 1).

Permeability, produced by volcanic and hydrothermal brecciation, provided the dominant control on the lateral extent and intensity of hydrothermal alteration. The matrices of permeable pyroclastic and

flow-top breccias commonly are strongly altered, whereas massive clasts within the breccias are weakly altered or unaltered. Dense interiors of lava flows and dikes adjacent to strongly altered breccias commonly are altered only along fractures. Most strongly altered clasts in clay-rich debris flows are fragments of breccias. These clasts are composed of variably altered massive fragments and matrices of altered glass and fine rock fragments. Some strongly altered breccia clasts in the Osceola Mudflow are hydrothermal breccias comprised of pervasively altered rock fragments containing pyrite-rich veinlets truncated at fragment margins in matrices of hydrothermal minerals or jigsaw breccia cemented by pyrite and silica phases (Fig. 7H).

Narrow zones of fracture-controlled alteration, including several types of veins, are visible locally in outcrop, most commonly where dikes intruded pyroclastic flows (Fig. 7E). In general veins are sparse, narrow, and discontinuous, and no silica mineral-rich veins or zones of stockwork veining have been found. Narrow (generally less than a few mm wide) pyrite veins are the most common vein type (Fig. 6B). In Glacier Basin, these veins also contain smectite. Irregular veins of anhydrite/gypsum up to several meters wide are exposed in the headwall of Sunset Amphitheater (Zimbelman, 1996; Zimbelman et al., 2005).

Leached and porous rocks with a skeletal texture are present locally, both around active fumaroles near the summit (Frank, 1985; Zimbelman, 1996; Zimbelman et al., 2000) and as clasts in several Holocene debris flows, including the Osceola Mudflow, the Paradise lahar, and the Tahoma Glacier rockfall. These rocks formed by intense acid alteration that left a residue of opal, kaolinite, alunite, and Fe- and Ti-oxide minerals.

6.2.4. Temperatures of hydrothermal alteration

Estimated temperatures of formation of hydrothermal alteration associations are listed in Table 1. Temperature constraints are provided by hydrothermal alteration mineralogy sampled by drill holes in other active hydrothermal systems (e.g., Henley and Ellis, 1983; Reyes, 1990; Simmons et al., 2005). Index minerals and mineral assemblages in these systems and found at Mount Rainier include: (1) the transition from smectite to mixed-layer illite/smectite at ~150 °C; (2) the transition of mixed-layer illite/smectite to illite at ~230 °C; (3) the limitation of kaolinite to temperatures ≤200 °C and dickite to temperatures of 150–300 °C; (4) the transition of kaolinite to pyrophyllite at temperatures >210 °C except at high silica activities; (5) the stability of illite at 230–270 °C; (6) the presence of chlorite at 150–350 °C; and (7) the formation of topaz generally at temperatures >200 °C. At Mount Rainier, pyrophyllite + opal-CT assemblages in single clasts from the Van Trump and Paradise lahars probably formed at ≤150 °C due to high silica activity, whereas pyrophyllite + quartz assemblages in the Osceola Mudflow likely formed at higher temperatures of 225–300 °C (Hemley et al., 1980). The absence of epidote in sparse chlorite altered clasts at Mount Rainier is evidence that temperatures in those rocks did not exceed about 240 °C.

6.3. Surface and subsurface distribution of hydrothermally-altered rocks

Only small areas of hydrothermally-altered Quaternary rocks are exposed on the surface of Mount Rainier, in part due to extensive snow and ice cover (Fig. 4). Much of the alteration shown in Fig. 4 is inhomogeneous and its area is exaggerated in size for display purposes. Exposed altered rocks are limited to three areas. The summit craters have been altered by the active hydrothermal system that post-dates the Osceola Mudflow (Frank, 1985). Discontinuous outcrops of older altered rocks form a narrow 12-km-long, east- to northeast-trending zone that divides the summit and is coincident with a corridor of dikes intruded during multiple periods of time (Fiske et al., 1963; Zimbelman, 1996; Crowley and Zimbelman, 1997; Bruce, 1998; Sisson et al., 2001). Altered rock also remains visible on the walls of the Osceola collapse crater.

Hydrothermally-altered rocks are divided into three intensity levels based on pervasiveness of alteration (Fig. 4). Strong intensity alteration is comprised of pervasively altered rocks, mostly of alteration associations 1, 3, 4, and 5. Exposures of this alteration are limited mostly to Sunset Amphitheater and the upper part of Puyallup Cleaver high on the upper west side of the edifice where dikes are abundant. Moderate intensity alteration generally is the smectite–pyrite association with local minor kaolinite and is typically restricted to breccia matrices. Where exposed in-situ, this intensity of alteration is confined to within 5 m of dike margins and to a vent complex along Puyallup Cleaver on the west side of the summit and along dike margins on the northeast side of the volcano near Glacier Basin. It probably also flanks the strong intensity alteration in Sunset Amphitheater, but this has not been verified by sampling due to hazardous and difficult access. Weak intensity alteration is gradational with moderate intensity alteration and contains sparse smectite ± pyrite that incompletely alters breccia matrices, lines vesicles, and coats fracture surfaces. Most of this alteration is in the east- to northeast-trending zone on both sides of the summit and in isolated small exposures on the east and southeast sides of the edifice. The weak intensity alteration imparts a brownish hue to outcrops, but volcanic glass is preserved within a few millimeters of clast and fracture surfaces. This lowest rank of alteration intensity affects the Steamboat Prow–Interglacier and Jeanette Heights areas on the lower northeast and west flanks of the volcano. Previous analysis of remote sensing images reported higher intensity advanced argillic alteration in those areas (Crowley and Zimbelman, 1997), but our field examination found that advanced argillic alteration is limited to Holocene debris-flow deposits mantling the ground surface.

Crowley and Zimbelman (1997) also imaged large areas of "vapor phase alteration" characterized by local goethite. Rocks in these areas are stained red to bright orange due to oxidation during cooling and degassing of the lava flows and breccias, with goethite deposited on fractures. No evidence supports formation of the iron oxides in response to circulation of sulfur-bearing hydrothermal fluids.

Finn et al. (2001) modeled the subsurface distribution of altered rocks using mapped surface alteration and detailed airborne geophysical surveys of the edifice. We infer that the modeled subsurface alteration they defined corresponds mostly to our areas of strong alteration. The models of Finn et al. suggest that altered rocks are confined largely to the summit area and to the east- to northeast-trending corridor through the summit. The greatest volume of altered rock lies beneath and east of Sunset Amphitheater on the west side of the summit, with several smaller volumes of altered rock lying along or near the walls of the Osceola collapse crater. The geophysical results show that the post-Osceola hydrothermal system has affected only the upper 20–50 m of rock beneath the summit. Finn et al. also modeled older alteration to ~1000 m depth beneath the summit and suggested that the volume of strongly altered rock is relatively small and discontinuously underlies an area <500 m wide.

6.4. Hydrothermal mineralogy of the F tephra

The F tephra erupted approximately simultaneously with formation of the Osceola Mudflow and contains a high abundance of clay minerals (Mullineaux, 1974; Vallance and Scott, 1997). Mullineaux ascribed the origin of the clay minerals to hydrothermal alteration of rocks within Mount Rainier prior to eruption of the tephra. Samples of the F tephra from Yakima Park and the head of Granite Creek (Fig. 5) examined in this study contain the same hydrothermal phases as the matrix of the Osceola Mudflow. Various forms of opaline silica are abundant in both deposits, but clay minerals and quartz are more abundant in the F tephra than in the Osceola Mudflow matrix. Pyrite is abundant in one sample of the tephra that was deposited on a water-saturated peat layer (Fig. 7A). Clay minerals in the tephra include smectite, kaolinite, pyrophyllite, and trace amounts of illite.

Table 2
Types and abundance of hydrothermal alteration associations in clay-rich Holocene debris flows from Mount Rainier

Debris flow	Age	Overall abundance of altered clasts[a]	Abundance of alteration associations		
	(y BP)		Common	Sparse	Rare
Van Trump lahar	~9500	Low	1		3,6
Osceola Mudflow (Main Fork lobe)	~5600	Moderate–High	1,3	8	4,5,6
Osceola Mudflow (West Fork lobe)	~5600	Moderate–High	1	3,5,6	2,7,9
Paradise lahar	~5600	Moderate	1,3	4	6
Round Pass lahar	~2600	Low	1		
Electron Mudflow (distal)	~550	Low	1		
Electron Mudflow (Emerald Ridge)	~550	Moderate	1		3,5
Tahoma Glacier rockfall	75–100	High	1	3	5

[a] Percent of total clasts in debris flow: low, <5 vol.%; moderate, 5–20 vol.%; high, >20 vol.%.

Hydrothermal phases identified by SEM and XRD in the sand and silt fraction of the F tephra include opal, quartz, rutile, topaz, alunite, and pyrite. Trace amounts of alunite crystals are irregularly shaped, possibly due to abrasion during transport and eruption. One alunite crystal is zoned compositionally with a Ca–P rich core consistent with woodhouseite. Topaz forms aggregates of euhedral crystals. Pyrite crystals typically are >10 μm in diameter and have euhedral to abraded morphologies; their $\delta^{34}S$ value (1‰) is consistent with $\delta^{34}S$ values of hydrothermal pyrites in altered clasts from the debris flows, and the lack of framboid textures support hydrothermal formation of this pyrite prior to eruption of the tephra.

6.5. Distribution of hydrothermal alteration associations in clasts in Holocene debris flows

The hydrothermal alteration-mineral associations identified in clasts vary significantly among the Holocene clay-rich debris flows (Table 2). Clasts in the Osceola Mudflow have all identified associations. Those in the Paradise lahar have associations 1, 3, 4, and 6, and the Tahoma Glacier rockfall clasts have associations 1, 3, and 5. The only sample for the Van Trump lahar contains associations 1, 3, and 6. Electron Mudflow clasts mostly are association 1, although sparse clasts of association 3 were detected in an outcrop at Emerald Ridge identified as the proximal Electron Mudflow. Other clay-rich debris flows have altered clasts limited to association 1.

Clay mineralogy varies consistently among debris-flow matrices and in the F tephra based on the XRD peak intensities of the <1 μm separates. Clays detected in the Electron Mudflow are mostly smectite with minor kaolinite and a trace of illite. Samples of this debris flow collected more than 10 km from the summit also have detectable chlorite that likely was incorporated from propylitically altered Tertiary bedrock as the flow moved down the mountain. The Paradise lahar contains abundant smectite with greater proportions of kaolinite than detected in the Electron Mudflow. The Osceola Mudflow samples are distinguished from the Paradise lahar by somewhat lower relative abundance of kaolinite and by the presence of pyrophyllite. Pyrophyllite abundance is markedly greater in the F tephra than in the Osceola Mudflow.

The distribution of alteration associations indicates that the Osceola Mudflow sampled higher temperature, deeper parts of the hydrothermal system(s), consistent with its much larger volume and the deeper downcutting of the northeast side of the edifice, as surmised by previous studies (Crandell, 1971; Scott et al., 1995; Vallance and Scott, 1997; Reid et al., 2001; Rye et al., 2003). Similarly, the eruption responsible for the F tephra exhumed fragments of hydrothermally-altered rocks from even deeper parts of the hydrothermal system. In contrast, the Paradise lahar, which formed by an avalanche of the south side of the volcano shortly prior to the Osceola Mudflow, only contains alteration minerals characteristic of the lower temperature shallow upper and outer parts of the Osceola hydrothermal system, as suggested by Vallance and Scott (1997). Successively younger debris-flow deposits (Round Pass Mudflow, Electron Mudflow, Tahoma Glacier rockfall) on the west side of the volcano have exposed progressively more strongly altered rocks. The early 20th century Tahoma Glacier rockfall contains alteration associations that have been detected only in the Osceola Mudflow and F tephra, suggesting that the headwall exposures in Sunset Amphitheater are approaching the core of alteration formed by an extinct hydrothermal system. The geophysical data and models of Finn et al. (2001) also support this interpretation.

Hydrothermal mineral associations in altered clasts also vary between the Main Fork and West Fork lobes of the Osceola Mudflow (Table 2). The West Fork lobe contains chlorite- and illite-rich clasts, dickite is present in some clasts, pyrophyllite is more common than in the Main Fork lobe, and alunite is more commonly part of magmatic-hydrothermal associations 5 and 6. In contrast, the Main Fork lobe contains more abundant alunite, mostly in steam-heated association 3, kaolinite is more common, and hypogene jarosite is present locally as part of association 4. These relations suggest that the West Fork lobe sampled rocks from deeper, higher temperature parts of the hydrothermal system, whereas the Main Fork lobe mostly sampled the upper and outer parts of the system.

7. Geochemistry of altered rocks and lahar matrices

7.1. Whole-rock compositions

Whole-rock chemical analyses of about 40 samples of altered clasts in debris flows, lahar matrices, and altered block and ash flows in Glacier Basin are summarized in Table 3. Most samples analyzed were smectite–pyrite altered clasts (20 samples) or bulk lahar matrix (10). Sulfur is the dominant element enriched during hydrothermal alteration. Altered rock clasts commonly contain 1–3 wt.% sulfur, with pyrite-rich samples containing up to 14 wt.%. Most other elements show little or no enrichment relative to typical calc-

Table 3
Summary of chemical analyses of altered rock and lahar matrix samples, Mount Rainier, WA. See Appendix A for analytical methods

Sample type[a]	1	4	5	9	10
No. samples	20	2	5	1	10
Total S (wt.%)[b]	0.9 (3.8)	(5.2)	5.8 (13.7)	0.46	1.2 (3.8)
Au (ppb)	<5 (20)	(0.5)	(9)	5	2.2 (33)
Hg (ppb)	25 (480)	(207)	30 (2560)	1250	60 (74)
As (ppm)	5 (13.8)	(34)	7.4 (50)	11	7.1 (19)
Bi	0.1 (1.1)	(0.1)	0.2 (10.3)	2.2	(3.2)
Cu	19 (46)	(42)	15 (33)	2.5	23 (37)
Mo	1.2 (2.3)	(0.7)	0.9 (8.8)	24.3	2.5 (7)
Pb	3.3 (17)	(2.9)	7.1 (27.7)	1.4	6.3 (12)
Sb	0.2 (0.9)	(0.3)	0.8 (6.4)	0.7	0.2 (0.6)
Se	0.7 (2.6)	(6.2)	(0.6)	na	1.5 (3)
Te	0.3 (1.2)	(4.4)	0.15 (0.8)	0.3	0.44 (0.7)
Zn	15 (63)	(8)	14 (60)	3	30 (47)

na, Not analyzed.
[a] 1–9, alteration associations 1 to 9 (Table 1); 10, lahar matrix.
[b] Median and maximum values.

alkaline andesites, and Cu, Pb, and Zn contents are generally lower than unaltered Mount Rainier andesite (Stockstill et al., 2002). All samples have low Au and Ag contents, generally <5 ppb and <1 ppm, respectively. A few smectite–pyrite altered rocks have weakly elevated values of As, Hg, Mo, and Se, although most samples show little enrichment in these elements. Some opal or quartz–pyrite–kaolinite ± alunite altered rocks are enriched in As, Bi, Hg, Mo, Pb, and Sb. Opal–alunite–jarosite altered rocks are enriched in As, Hg, Se, and Te. Lahar matrix samples are enriched in sulfur (see next section) and commonly are weakly enriched in As and Mo. These limited data indicate pronounced sulfur metasomatism but little to no enrichment of other metallic elements common in porphyry copper and high-sulfidation epithermal systems related to calc-alkaline magmatism (e.g., Ag, Au, Cu, Mo, Pb, Zn).

7.2. Sulfur contents and sulfur speciation of lahar matrices

Total sulfur contents in the −10 mesh (<2 mm) fraction measured for 80 samples of clay-rich debris flows, tephras, and glacial tills vary among sample types. Concentrations range from 0.01 to 4.78 wt.% with the lowest values (<0.07 wt.%) in glacial tills representative of average degassed Mount Rainier volcanic rocks. Generally high sulfur contents (>0.2 wt.%) are characteristic of samples from the Osceola and proximal Electron Mudflows, Paradise and Van Trump lahars, and Tahoma Glacier rockfall. Low sulfur contents are characteristic of the Reflection Lakes lahar and Round Pass and distal Electron Mudflows. Progressive incorporation of unaltered exotic rock fragments into a lahar along its path, known as bulking, dilutes the sulfur content. Such dilution might account for the large difference in sulfur concentration between the proximal and distal parts of the Electron Mudflow deposit. A similar decrease apparent in samples of the Osceola Mudflow has a more complicated explanation, which includes bulking, heterogeneity of alteration with the initial avalanche mass, and post-depositional weathering. Within the Osceola, axial deposits consistently contain greater amounts of sulfur (up to 4.78 wt.%) and lower proportions of unaltered eroded sediment (bulking of 40–60%; Vallance and Scott, 1997) than those higher on the valley side (0.03–0.06 wt.% sulfur and bulking of 80–90%). Such a two-to-one factor in bulking clearly can explain only part of the contrast in sulfur content. The lower sulfur content in marginal valley-side deposits is consistent with a suggestion advanced in Vallance and Scott (1997) that such deposits came from the outermost, least altered part of the edifice before its failure and, after the edifice collapse, this less-altered rock became the lead edge of the debris flow and was subsequently deposited at inundation limits and high on valley sides. Lastly, low sulfur contained in valley-side deposits may have resulted from leaching of sulfur during weathering of these relatively thin deposits. Prior to weathering and leaching of sulfur, the total sulfur content of the Osceola Mudflow is estimated at about 90 million tonnes (Mt), assuming a volume of 3.8 km^3, 40 vol.% matrix (sand, silt, and clay-sized fragments) that contains 2 wt.% sulfur and 60 vol.% clasts containing 0.5 wt.% sulfur, and an overall average density of 2.5 g/cc.

Surficial exposures of the lahars are typically pale yellow-brown (Fig. 7F). Shallow excavation yields material that is purple-gray with ferric oxyhydroxides coating fractures. Water-saturated intervals are distinctly massive and dark gray (Fig. 7G). Oxidation of pyrite and dissolution of soluble sulfate minerals likely resulted in loss of sulfur to surface water flowing through the debris flows. The progressive decrease in sulfur concentrations toward the surface in exposures of the Osceola Mudflow at Interfork, Buck Creek, and Greenwater results from sulfur loss caused by weathering (Table 4).

The forms of sulfur in the matrices vary among debris flows. Sequential extraction of one sample of the Round Pass deposit on the west side of Mount Rainier (Table 4) contained water-soluble sulfate (anhydrite/gypsum), supergene jarosite, and pyrite. Similarly, the Reflection Lakes lahar and Round Pass and distal Electron Mudflows lack detectable alunite consistent with the dominance of smectite–pyrite alteration in these debris flows. In contrast, alunite is present in

Table 4
Summary of the results of total sulfur and sulfur speciation analyses of selected matrix samples (−10 mesh) from Mount Rainier debris flows. Speciation determined by the sequential extraction method of Berry and Breit (2007). Depth below ground surface is listed for samples collected in a vertical sequence from cutbanks along the White River. (nd, Not determined; *, water-saturated sample)

Sample number	Debris-flow-location	Depth below ground surface	Distance to summit	Total sulfur	Elemental sulfur	Water soluble	Supergene jarosite	Pyrite	Alunite	Residual
		(m)	(km)	(wt.%)	(Rel. %)	(Rel. %)	(Rel. %)	(Rel. %)	(Rel.%)	(Rel.%)
Osceola Mudflow										
Main Fork White River										
MR-05-06	Osceola—Steamboat Prow	–	3.5	0.54	<1	<1	7	<1	69	20
MR-05-04	Osceola—Mount Ruth	–	4	0.85	1	1	1	<1	73	25
MR-02-16	Osceola—Glacier Basin	–	6	0.28	1	2	17	1	71	7
06-RN-05*	Osceola—Glacier Basin	–	6	4.3	<1	26	1	64	3	5
MR-02-63	Osceola—Interfork	10	9	0.51	1	2	38	1	55	4
MR-02-64	Osceola—Interfork	20	9	0.93	<1	1	39	1	57	2
MR-02-43	Osceola—Buck Creek	1	25	0.40	2	6	56	1	32	3
MR-02-44	Osceola—Buck Creek	3	25	0.66	1	5	56	1	34	3
MR-04-03	Osceola—Dalles Camp.	2	28	0.42	1	1	62	1	31	5
MR-04-02	Osceola—Dalles Camp.	3	28	0.31	2	1	87	1	3	6
MR-02-34	Osceola—Greenwater	2	34	0.39	Nd	nd	nd	nd	nd	nd
MR-02-36	Osceola—Greenwater	4	34	0.74	1	23	47	10	16	3
MR-02-38	Osceola—Greenwater	7	34	1.13	Nd	nd	nd	nd	nd	nd
West Fork White River										
MR-05-10*	Osceola—Winthrop Glacier	–	10	2.3	<1	4	<0.5	92	5	<1
MR-05-12	Osceola—Winthrop Glacier	–	10	0.23	<2	<2	16	22	4	35
MR-04-04	Osceola—FR74	1.5	29	0.38	2	9	72	7	5	5
MR-04-05*	Osceola—FR74	2.5	29	1.84	<1	10	26	65	<1	1
02-RN-39*	Osceola—FR74	–	29	0.71	2	18	38	51	<1	3
Other lahars										
MR-04-01	Van Trump—V. Trump Park	–	6	0.20	1	0	45	2	41	10
MR-04-10	Round Pass—Deer Creek	–	16	0.05	8	13	30	11	<1	43
06-RN-02*	Paradise—Myrtle Falls	–	7	2.2	<1	4	1	80	18	5
OORE-854	Paradise—Parking lot	–	8	0.50	<1	<1	<1	<1	96	4
OORE-856	Paradise—Ricksecker Point	–	9	1.00	1	<1	<1	<1	97	2

the Paradise and Van Trump lahars and in some Osceola samples (Tables 4 and 5).

8. Stable-isotope studies

Light stable-isotope (O, H, S, C) compositions were measured for hydrothermal minerals, altered rocks, and lahar matrices from Mount Rainier to help identify fluid sources and environments of hydrothermal alteration. Sample locations are shown in Fig. 5, and analytical methods are described in the Appendix. The stable-isotope data for sulfur-bearing and hydrous minerals in clasts in various debris flows are summarized in Tables 6 and 7, respectively. The S and O isotope data for supergene and hypogene anhydrite/gypsum, alunite, and jarosite are plotted in Fig. 8, with reference fields from Rye et al. (1992). The H and O isotope data for hydrous minerals are plotted in Fig. 9.

8.1. S isotopes

We divide samples of anhydrite/gypsum and jarosite into groups with hypogene and supergene origins on the basis of petrographic characteristics. Gypsum crystals are considered hypogene if they contain anhydrite and/or pyrite inclusions, fill narrow veins (commonly with pyrite), or replace igneous phenocrysts, whereas fine-grained crystals intergrown with Fe-oxides or late vug fillings are considered supergene. Similarly, crystalline jarosite cementing breccias is identified as hypogene, whereas fine-grained earthy jarosite and amorphous jarosite coating fractures in oxidized rocks are interpreted to have a supergene origin. All analyzed alunite samples are considered hypogene on the basis of their petrographic characteristics (Fig. 6).

The sulfate minerals have an exceptionally broad range of S and O isotope compositions (Fig. 8). This range indicates distinctly different hydrothermal environments (magmatic-hydrothermal, steam-heated, and magmatic steam) of formation for sulfate minerals within the pre-Osceola collapse edifice, and the formation of supergene sulfates in the debris flows after edifice collapse. The S and O isotope results for the hypogene sulfates define two trends (see shaded areas of Fig. 8) of increasing $\delta^{34}S$ with increasing $\delta^{18}O_{SO_4^{2-}}$. One of these trends has large $\delta^{18}O_{SO_4^{2-}}$ values that extend upward from $\delta^{18}O_{SO_4^{2-}}$ and $\delta^{34}S$ values typical of magmatic steam alunite. The other trend has lower $\delta^{18}O_{SO_4^{2-}}$ values, ranging from values typical of steam-heated alunite to those typical of magmatic-hydrothermal alunite. At low $\delta^{34}S$ values of the two trends, there is a continuous range of $\delta^{18}O_{SO_4^{2-}}$ values. Samples with the greatest $\delta^{18}O_{SO_4^{2-}}$ values were collected from the Paradise lahar and the Main Fork lobe of the Osceola Mudflow, whereas samples on the lower $\delta^{18}O_{SO_4^{2-}}$ trend are mostly from both the Main Fork and West Fork lobes of the Osceola Mudflow and from the Tahoma Glacier rockfall.

8.1.1. Supergene sulfates

The S and O isotopic composition of supergene sulfates differ from hypogene sulfates, such that supergene sulfates have the lowest $\delta^{34}S$ and $\delta^{18}O_{SO_4^{2-}}$ values (Fig. 8). Our analyses indicate that supergene sulfates are jarosite and gypsum whose parent aqueous sulfate is attributed to the low-temperature oxidation of pyrite in pyrite–smectite altered rocks. As expected, the $\delta^{34}S$ values of these supergene sulfates overlap with values for pyrite. The $\delta^{18}O_{SO_4^{2-}}$ values of supergene sulfates range from +5 to −8‰, reflecting the variable contributions of meteoric water and atmospheric oxygen in parent aqueous sulfate (Taylor et al., 1984; Rye et al., 1992) that are likely during oxidation within the debris-flow deposits and on the edifice prior to collapse.

Table 5
Number of samples that contained detectable amounts of selected alteration minerals as determined by X-ray diffraction of the −10 mesh fraction of debris-flow and F tephra samples. (*n*, total samples analyzed)

Unit	*N*	Quartz	Pyrite	Jarosite	Alunite	Gypsum	Kaolinite
Electron Mudflow	5	1	0	0	0	0	0
Round Pass lahar	5	2	0	0	0	0	0
Osceola Mudflow	30	29	4	7	1	4	11
Paradise lahar	10	0	1	0	6	0	4
Reflection Lakes lahar	4	0	0	0	0	0	0
Van Trump lahar	1	0	0	0	0	0	1
F tephra	7	7	1	1	0	1	2

8.1.2. Magmatic-hydrothermal sulfates

Magmatic-hydrothermal sulfate is derived from H_2SO_4 generated from the disproportionation of magmatic SO_2 during condensation of magmatic vapor below 400 °C. When magmatic vapor condenses in meteoric water, low $\delta^{18}O_{SO_4^{2-}}$ values may result (Rye et al., 1992). A diagnostic feature of alunites formed in this environment is their coexistence with pyrite and $\delta^{34}S$ values that reflect sulfur isotope equilibrium between oxidized and reduced aqueous sulfur species in their parent fluids. Because evolved magmatic fluids in volcanic systems like Mount Rainier typically have H_2S/SO_2 values greater than 1 (Arribas, 1995; Rye, 1993, 2005), the $\delta^{34}S$ values of the pyrite are close to that of the bulk sulfur in the fluid, whereas $\delta^{34}S$ values of the alunite are characteristically much higher and have a larger variation (Table 6). Most of the alunite and pyrite in samples analyzed for Table 6 may not be contemporaneous and therefore not in equilibrium. Nevertheless, the pyrite–alunite sulfur isotope fractionations in two samples (04-RN-3C, 05-RN-17Q) give reasonable temperatures of about 225 °C and 260 °C, respectively, using the equilibrium fractionation factors of Ohmoto and Rye (1979).

8.1.3. Steam-heated sulfates

The aqueous sulfate available to form shallow sulfate minerals in steam-heated environments is derived from atmospheric oxidation of H_2S. The $\delta^{34}S$ value of the sulfate in the steam-heated environment is typically close to the value for H_2S, because $SO_4^{=}$–H_2S exchange is slow at low temperatures. Partial exchange with H_2S resulting in larger $\delta^{34}S$ values for parent aqueous sulfate may occur depending on its residence time prior to precipitation as a sulfate mineral. The $\delta^{18}O_{SO_4^{2-}}$ values may vary depending on the proportions of ^{18}O-enriched atmospheric oxygen ($\delta^{18}O = 23‰$) or ^{18}O-depleted meteoric water incorporated in the aqueous sulfate. The $\delta^{18}O_{SO_4^{2-}}$ values likely to form in the steam-heated sulfates on Mount Rainier are lower than the values for the steam-heated reference composition (Fig. 8; Rye et al., 1992). These low values likely are due to the incorporation of oxygen from low ^{18}O meteoric water derived from glacier melt on the edifice of Mount Rainier.

8.1.4. Magmatic steam alunite and jarosite

Alunite, jarosite, and anhydrite/gypsum in some variably altered clasts collected in the Paradise lahar and Osceola Mudflow on the lower edifice flanks (Paradise Park and Mt. Ruth, respectively, Fig. 5) have high $\delta^{18}O_{SO_4^{2-}}$ values and show a positive $\delta^{34}S$ vs. $\delta^{18}O_{SO_4^{2-}}$ trend (Fig. 8). These alteration features probably formed near eruptive vents high on the edifice where volcanic fluids discharged with little interaction with snowmelt. Aqueous sulfate in these minerals formed during the rapid expansion of high-temperature SO_2-rich magmatic fluid such that sulfur isotope equilibrium between reduced and oxidized sulfur species formed during disproportionation of SO_2 was not maintained. Sulfate minerals with similarly high $\delta^{18}O_{SO_4^{2-}}$ values have been measured from other stratovolcanoes (Zimbelman et al., 2005) and are interpreted here as the result of ^{18}O-enrichment during separation of vapor and/or exchange with isotopically heavy atmospheric oxygen ($\delta^{18}O = 23‰$) that was entrained in the degassing magmatic fluid in an open vent near the paleosurface of the pre-collapse edifice.

Table 6
Sulfur and oxygen isotope analyses of sulfur phases in samples from Mount Rainier. See Appendix A for analytical techniques and precision

Sample number	Sample type	Location	Alteration type[a]	Elemental S $\delta^{34}S$	Gypsum/anhydrite $\delta^{34}S$	Gypsum/anhydrite $\delta^{18}O$	Jarosite $\delta^{34}S$	Jarosite $\delta^{18}O$	Pyrite $\delta^{34}S$	Alunite–barite $\delta^{34}S$	Alunite–barite $\delta^{18}O$
				(‰)	(‰)	(‰)	(‰)	(‰)	(‰)	(‰)	(‰)
Electron Mudflow											
MR-02-01	Clast	Emerald Ridge	1	2.7	2.7	1.0	0.9	nd	−0.5		
MR-02-10	Clast	Emerald Ridge	1	0.8	0.1	−1.4	1.3	nd	−0.9		
MR-02-07	Matrix	Emerald Ridge	Mixed				1.6	−3.3			
Paradise lahar											
03-RN-09	Clast	Ricksecker Point	3							4.1	16
02-RN-34*	Clast	Paradise Park	4				4.2	11.6			
Paradise	Clast	Paradise Park	4	6.4	4.7	4.5				7.1	nd
Paradise*	Clast	Paradise Park	4				3.8	13.2			
MR-02-59A	Clast	Paradise Park	4	9.5	7.6	14.9				10.5	15.9
06-RN-02	Matrix	Myrtle Falls	Mixed		−1.5		−1.1		0.1	13.1	
00-RE-854	Matrix	Paradise	Mixed							2.1	3.2
00-RE-856	Matrix	Ricksecker Point	Mixed							7.7	0.0
Osceola Mudflow											
05-RN-11A	Clast	Mount Ruth	3	2.4						15.6	20.5
05-RN-11B	Clast	Mount Ruth	3							15.4	20.6
05-RN-11C	Clast	Mount Ruth	3						−7.0	15.5	19.4
05-RN-12E	Clast	Mount Ruth	3	3.2					0.4	5.4	nd
05-RN-12I	Clast	Mount Ruth	4		5.5	nd	5.0	9.1		6.7	14.3
05-RN-12K	Clast	Mount Ruth	6	9			3.5	−1.9	1.4		
05-RN-12P	Clast	Mount Ruth	3	6.7	5.7	−1	4.4	−0.4	2.2		
MR-05-05	Clast	Mount Ruth	1	−0.2	4.6	5.2	−1.4	nd	−3.6		
MR-02-13	Clast	Glacier Basin	3							5.7	6.5
MR-02-15	Clast	Glacier Basin	1	−0.3	−0.4	−7.1	1.2	nd	−0.3		
MR-02-17	Clast	Glacier Basin	1	7.8	−0.5	nd			−1.5		
02-RN-15	Clast	Glacier Basin	?						−1.7		
MR-02-68	Clast	Interfork	1	2.4			2.9	nd	−2.2		
02-RN-27	Clast	Greenwater	5	−3.3	3.4	2.3	−3.6	5.5	−8.8	5.3	13.5
03-RN-10A	Clast	Greenwater	5		10.2	4.9			−0.7	13.3	12.4
03-RN-10D	Clast	Greenwater	6		11.3	5.4	−4.3	nd	−5.1		
03-RN-10E	Clast	Greenwater	3	3.3	7.2	3.9			1.2		
MR-02-37A	Clast	Greenwater	1	2.9	10.3	5.8			−1.6		
Greenwater-1	Clast	Greenwater	1	1.8	1.8	−4.5	2.1	nd	1.6		
04-RN-03c	Clast	West Fork	5		−0.4	−5.3			−2.1	16.4	9.2
05-RN-17A	Clast	Winthrop Glacier	3		1.4	−4.3	1	0	1.8		
05-RN-17J	Clast	Winthrop Glacier	6		−1.2	nd	−1.2	−3.1	−3.1		
05-RN-17Q	Clast	Winthrop Glacier	6				0.6	1.1	−4.1	20.7	12.0
05-RN-17R	Clast	Winthrop Glacier	6						−2.5		
MR-02-16	matrix	Glacier Basin	mixed	2.4	2.3	0.4	2.3	−2.4			
06-RN-05	matrix	Glacier Basin	mixed		14.2				1.7		
MR-02-63	matrix	Interfork	mixed	−0.1	1.4	−7.2	1.8	−5.3			
MR-02-64	matrix	Interfork	mixed	4.0	3.8	−5.4	3.5	−5.7			
MR-02-42	matrix	Buck Creek	mixed	5.3	3.3	−4.9	2.4	−3.0	0.2		
MR-02-44	matrix	Buck Creek	mixed	2.9	3.1	−4.9	2.6	−3.2			
MR-02-36	matrix	Greenwater	mixed	3.5	0.8	−6.0	0.8	−4.1	1.2		
MR-02-38	matrix	Greenwater	mixed		1.5	−4.0	1.2	−2.6	1.5		
02-RN-39	matrix	West Fork	mixed	1.6	0.6	−4.6	1.4	−3.1	0.1		
MR-04-04	matrix	West Fork	mixed						−2.7		
MR-04-05	matrix	West Fork	mixed						−0.7		
Tahoma Glacier											
02-RN-03	clast	Tahoma Glacier	1		10.9	4.6	6.1	nd	2.1		
02-RN-04	clast	Tahoma Glacier	1	5.5	7.0	0.0			−0.4		
02-RN-05	clast	Tahoma Glacier	1	8.7	2.9	−6.8	2.6	−4	2.5		
02-RN-6B	clast	Tahoma Glacier	5	2.6	0.4	1.0	0.2	3.5	−1.9		
02-RN-10	clast	Tahoma Glacier	5		12.0	6.2			1.0	12.4	7.5
Other											
GB Dike	outcrop	Glacier Basin	1		2.5	−4.1	2.4	−4.6	2.5		
JV-637	matrix	F-tephra	mixed						−0.6		
MR-02-27	matrix	F-tephra	mixed		−6.0	nd			−0.3		

Phases were extracted using the procedure of Berry and Breit (2007) unless otherwise indicated. nd=not determined.
[a] Alteration associations in Table 1.

8.1.5. Elemental sulfur

Many debris-flow clasts contain elemental sulfur that has $\delta^{34}S$ values 1 to 9‰ higher than $\delta^{34}S$ values of pyrite in the same sample (Fig. 10, Table 6). Clearly, pyrite and elemental sulfur did not form in sulfur isotopic equilibrium, consistent with the typical occurrence of elemental sulfur in vugs and following pyrite in the paragenesis of each clast. Because sulfur precipitated later than pyrite, its higher $\delta^{34}S$ values may reflect the evolution of the isotopic composition of bulk sulfur during progressive degassing of one or more batches of magma. Magmas that feed Mount Rainier and similar Cascades arc andesitic

Table 7
Oxygen and hydrogen isotope analyses of hydrous minerals in samples from Mount Rainier. See Appendix A for analytical techniques and precision

Sample number	Sample type	Location	Alteration type[a]	Mineral	Temperature[b]	Measured values		Calculated water	
						$\delta^{18}O$	δD	$\delta^{18}O$	δD
					(°C)	(‰)	(‰)	(‰)	(‰)
Electron Mudflow									
MR02-02	Clast	Emerald Ridge	1	Smectite	125	8.3	−91	−3.0	−71
Osceola Mudflow									
05RN 12K	Clast	Mt. Ruth	6	Pyrophyllite	275	9.5	−84	3.7	−64
05RN 17J	Clast	Winthrop Glacier	6	Pyrophyllite	275	11.1	−92	5.3	−72
05RN 17Q	Clast	Winthrop Glacier	6	Pyrophyllite	250	10.3	−87	3.5	−67
05RN 17R	Clast	Winthrop Glacier	6	Pyrophyllite	250	10.1	−83	3.3	−63
05-RN-12P	Clast	Mt. Ruth	5	Kaolinite	175	7.7	−119	0.7	−100
05-RN-17A	Clast	Winthrop Glacier	5	Kaolinite	175	7.7	−117	0.7	−98
MR02-13	Clast	Osceola clast	3	Alunite	125	6.5	−125	−10.1	−119
05RN-12I	Clast	Mt. Ruth	3	Alunite	150	14.3	−90	0.0	−84
05RN-11A	Clast	Mt. Ruth	3	Alunite	150	20.5	−58	6.2	−52
05RN-11B	Clast	Mt. Ruth	3	Alunite	150	20.6	−62	6.3	−56
05RN-17Q	Clast	Winthrop Glacier	6	Alunite	250	12.0	−73	3.6	−67
MR02-37	Clast	Glacier Basin	1	Smectite	150	7.1	−99	−2.5	−79
05RN-12F	Clast	Mt. Ruth	1	Smectite+mica	175	7.4	−103	−0.7	−83
05RN-17N	Clast	Winthrop Glacier	2	Chlorite+I/S	200	3.9	−97	−1.2	−67
05RN-17Y	Clast	Winthrop Glacier	2	Mica+chlorite	225	4.3	−98	0.3	−69
Paradise lahar									
MR02-59A	Clast	Paradise Park	3	Alunite	125	15.9	−75	−0.7	−69
02-RN-34	Clast	Paradise Park	4	Jarosite	125	13.2	−141	−2.2	−81
Paradise	Clast	Paradise Park	4	Jarosite	125	11.6	−135	−3.8	−75
Glacier Basin dike wall rock[c]									
GB-002	Outcrop	Glacier Basin	1	Illite–smectite (30% I)	150	3.9	−145	−5.7	−125
GB-037	Outcrop	Glacier Basin	1	Illite–smectite (20% I)	150	5.8	−97	−3.8	−77
GB-033	Outcrop	Glacier Basin	1	Smectite	125	5.6	−136	−5.7	−116
GB-038	Outcrop	Glacier Basin	1	Smectite	125	5.7	−141	−5.6	−121

[a] Table 1.
[b] Estimated temperature of formation (±25 °C); see text for temperature constraints on alteration associations.
[c] Samples from Bruce (1998).

volcanoes ultimately originate in the mantle and undergo differentiation and assimilation processes at lower to mid-crustal depths (e.g., Hildreth, 2007). At Mount Rainier the resulting magmas ascend typically in small batches, and last stagnate in sizeable amounts probably at 8 or more km depth before erupting. Mount Rainier magmas commonly have oxidation states 1 to 2 log units above the Ni–NiO buffer, and at the pressure of the probable storage depths, the exsolved magmatic fluid would be H_2S rich, such as calculated for the 1982 eruption of El Chichon (Luhr et al., 1984). Because of fractionation between reduced and oxidized sulfur species in magmas (Ohmoto and Rye, 1979; Rye, 2005), the early loss of H_2S increases the $\delta^{34}S_{\Sigma S}$ value of residual magma raising $\delta^{34}S$ values for subsequently released H_2S. During the waning stages of a magmatic event, progressive degassing of magmas stalled in the mid to upper crust would lead to progressively higher $\delta^{34}S$ values in degassing fluids coupled with decreasing alteration temperatures, as recorded by precipitation of pyrite followed by elemental sulfur at temperatures <120 °C in the debris-flow clasts.

8.2. H–O isotopes

The H and O isotopic data for alunite, jarosite, kaolinite, pyrophyllite, chlorite, illite, and smectite in debris-flow clasts and for a few samples of smectite from outcrops in Glacier Basin are plotted in Fig. 9. The isotopic compositions of water in parent fluids calculated using probable formation temperatures (Table 7) also are plotted. These parent waters are considered relative to the range of isotopic compositions of meteoric water on Mount Rainier (Frank, 1995). The large range of values reflects an approximate δD gradient of 65‰ per kilometer of elevation. Although smectite is the most common hydrous mineral produced by

Table 8
Isotope fractionation equations used in this study

Element-fractionation equation	Isotope	Temperature range	Reference
		(°C)	
$10^3\ln\alpha_{kaolinite-H_2O} = 2.76\times10^6T^{-2} - 6.75$	Oxygen	0–350	Sheppard and Gilg (1996)
$10^3\ln\alpha_{pyrophyllite-H_2O} = 2.76\times10^6T^{-2} + 1.08\times10^3T^{-1} - 5.37$	Oxygen	0–700	Savin and Lee (1988)
$10^3\ln\alpha_{illite-muscovite-H_2O} = 2.39\times10^6T^{-2} - 3.76$	Oxygen	0–700	Sheppard and Gilg (1996)
$10^3\ln_{alunite\ (SO4)}\times10^6 - 2.94$	Oxygen	250–450	Stoffregen et al. (1994)
$10^3\ln\alpha_{chlorite-H_2O} = 2.69\times10^9T^{-3} - 6.34\times10^6T^{-2} + 2.97\times10^3T^{-1}$	Oxygen	170–350	Cole and Ripley (1999)
$10^3\ln\alpha_{kaolinite-H_2O} = -2.2\times10^6T^{-2} - 7.7$	Hydrogen	0–300	Sheppard and Gilg (1996)
$10^3\ln\alpha_{pyrophyllite-H_2O} = -20\pm5$	Hydrogen	120–400	Marumo et al. (1980)
$10^3\ln\alpha_{illite-muscovite-H_2O} = -20\pm5$	Hydrogen	120–400	Marumo et al. (1980)
$10^3\ln\alpha_{alunite-H_2O} = -6$	Hydrogen	250	Stoffregen et al. (1994)
$10^3\ln\alpha_{chlorite-H_2O} = -3.7\times10^6T^{-2} - 24$	Hydrogen	500–700	Graham et al. (1984)

Note: The hydrogen isotope fractionation factor of muscovite (Marumo et al., 1980) was used for pyrophyllite because of the lack of experimental data.

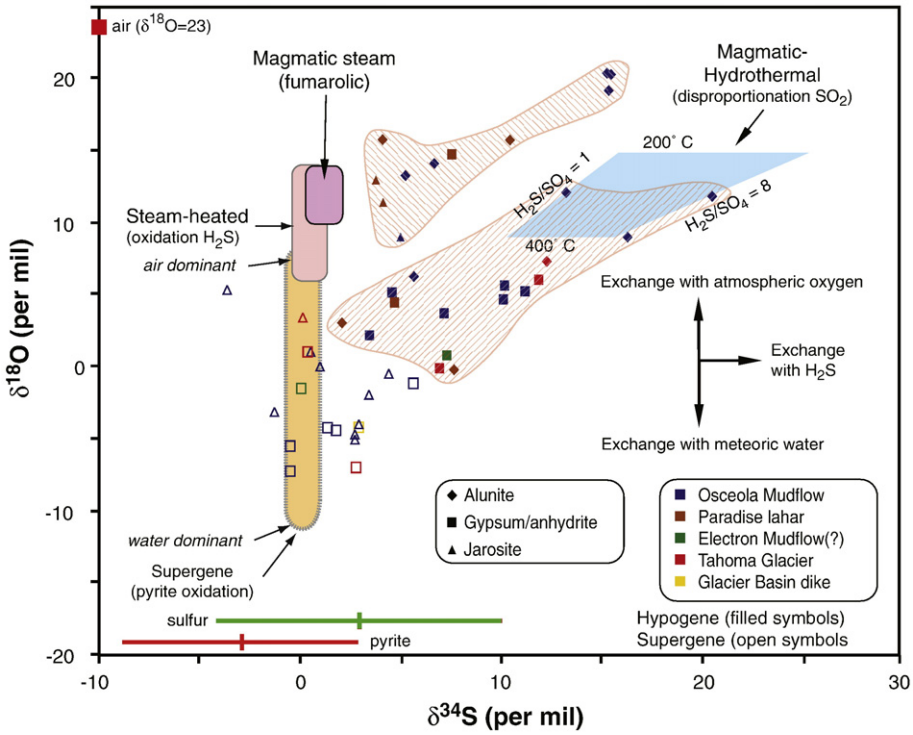

Fig. 8. S and O isotope data for supergene (open symbols) and hypogene (closed symbols) sulfate minerals from various debris flows on Mount Rainier. Bars in lower left corner show range and median $\delta^{34}S$ values for pyrite and elemental sulfur. Reference fields are from Rye et al. (1992) and are the predicted S and O isotope composition of alunite in supergene, steam-heated, magmatic steam and magmatic-hydrothermal environments for the following assumptions: $\delta^{34}S_{\Sigma S}$=0‰ for all fluids, $\delta^{18}O_{H_2O}$=−5 and −15‰ for exchanged and unexchanged meteoric water fluid, respectively, and $\delta^{18}O_{H_2O}$=6‰ for magmatic fluids. The magmatic-hydrothermal reference is defined for alunites derived from such parent fluids at temperatures of 200–400 °C and H_2S/SO_4 ratios of 1 to 8. The range of $\delta^{18}O_{SO_4}$ values for steam-heated and supergene sulfate derives from the relative contributions of atmospheric oxygen and meteoric water oxygen to the parent aqueous sulfate. The horizontal arrow shows the direction of change in $\delta^{34}S$ of the aqueous sulfate derived from the disproportionation of magmatic SO_2 when it undergoes exchange with H_2S, while the vertical arrow shows the direction of change in $\delta^{18}O_{SO_4}$ when the aqueous sulfate exchanges in meteoric water (downward) or with atmospheric oxygen (upward). See Rye et al. (1992) for further details. All of the reference fields for alunite are applicable to the Mount Rainier sulfate samples except, perhaps, the one for stream-heated alunite that should probably extend to lower $\delta^{18}O_{SO_4}$ values to accommodate the possible influence of isotopically light meteoric water derived from the glacial melt waters.

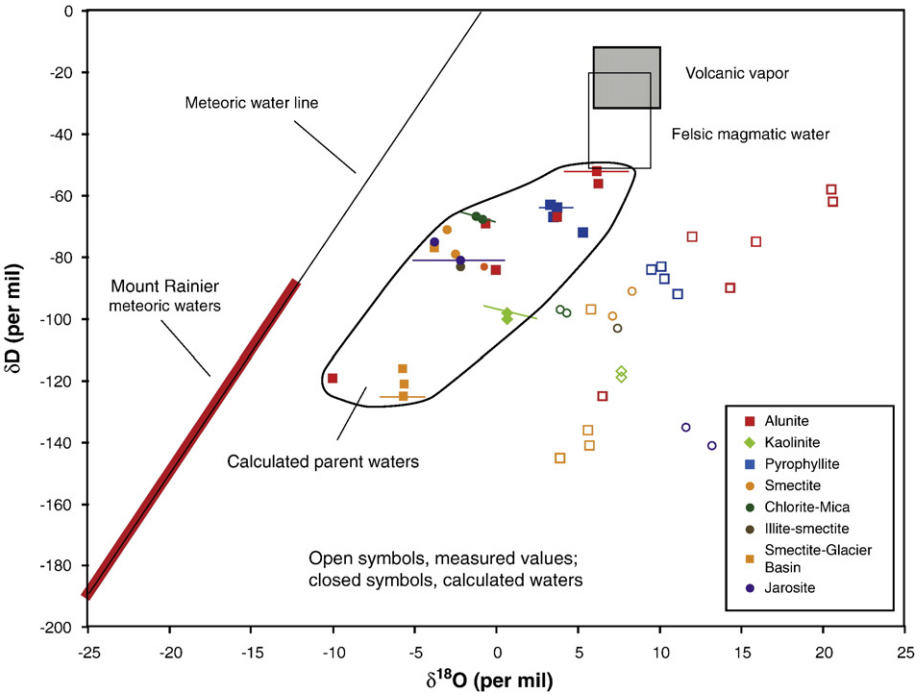

Fig. 9. Plot of hydrogen and oxygen isotopic data for clay minerals, alunite, and jarosite and calculated parent water compositions for Mount Rainier samples (Table 7). Water compositions calculated at estimated formation temperatures (Table 7) and fractionation factors listed in Table 8. Bars show range of calculated water compositions at ±25 °C of estimated temperatures of formation for each mineral. Meteoric water line is from Craig (1961), and meteoric water compositions at Mount Rainier are from Frank (1995). Volcanic vapor and felsic magmatic water boxes from Giggenbach (1992) and Taylor (1992), respectively.

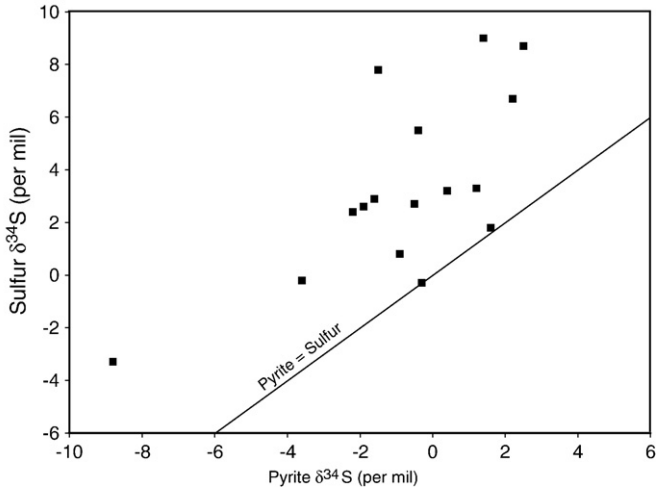

Fig. 10. Plot of $\delta^{34}S$ values of coexisting pyrite and later elemental sulfur from debris-flow clasts showing that elemental sulfur always has the larger value.

hydrothermal alteration on Mount Rainier, it is susceptible to post-depositional isotope exchange with later fluids (O'Neil and Kharaka, 1976). Therefore, most of our analyses were on alunite, pyrophyllite, kaolinite, chlorite, and jarosite that are more reliable indicators of the history of hydrothermal alteration fluids.

The striking linear trend of H and O isotopic composition of water in calculated parent hydrothermal fluids (Fig. 9) is similar to those that have long been recognized in studies of hydrothermal systems and ore deposits and is best explained by mixing of water in fluids from magmatic and meteoric sources. The fluids with the largest magmatic component are those associated with most alunites and pyrophyllites. The parent fluids for coexisting alunite and pyrophyllite from the same clast (05-RN-17Q) in the Osceola Mudflow have nearly identical calculated $\delta^{18}O_{H_2O}$ and δD values and are consistent with a magmatic water source. With one exception (alunite MR02-13), fluids calculated from smectite and kaolinite have the largest meteoric water component and the largest deviations in δD values from a tight linear trend. These deviations are consistent with post-formation isotopic exchange with meteoric water (O'Neil and Kharaka, 1976). Consistent with such exchange, the smectite in outcrops in Glacier Basin have lower δD values than the smectite occurring in nearby debris-flow clasts (Table 7). The exchange results in calculated δD values for the water of formation that are lower than the actual parent fluids.

The calculated H and O isotopic compositions of water in parent fluids of alunites encompass the range of compositions for all hydrous minerals. The alunites with the largest $\delta^{18}O_{SO_4 2-}$ values are interpreted to have formed in a magmatic steam environment in fumaroles at the summit of the pre-Osceola edifice. One alunite whose $\delta^{34}S$ and $\delta^{18}O_{SO_4^{2-}}$ values indicate a magmatic-hydrothermal origin has a calculated parent water δD value of −67‰ consistent with a substantial magmatic water component. The isotopically lightest calculated water in the parent fluids (Fig. 9) is from alunite in a clast in the Osceola Mudflow (MR-02-13) that also has the lowest $\delta^{18}O$ and $\delta^{34}S$ values, consistent with its formation in a steam-heated environment in which aqueous sulfate is derived largely from the oxidation of H_2S in near-surface meteoric water.

9. Discussion and model for hydrothermal systems on Mount Rainier

9.1. Hydrothermal environments at Mount Rainier and a model for the pre-Osceola Mudflow hydrothermal system

Hydrothermal–mineral associations, rock textures, and stable stable-isotope compositions of hydrothermal minerals indicate that hydrothermal alteration formed in a variety of environments ranging from steam-heated and magmatic steam, similar to those presently active near the summit, to the deeper magmatic-hydrothermal environment sampled by the Osceola Mudflow and the F tephra (Table 1). Our model for the distribution of hydrothermally-altered rocks on Mount Rainier at about 5600 y BP, shortly prior to eruption of the F tephra and formation of the Osceola Mudflow (Fig. 11), is constrained by (1) exposures of hydrothermally-altered rocks on the modern edifice, (2) distribution of alteration-mineral associations in debris flows, (3) hydrothermal environments and sources of hydrothermal components inferred from alteration-mineral associations, mineral stability relations, and stable-isotope data, (4) permeability controls on alteration, including presence of breccia units, primary dips, local aquifers, and fractures and dikes, (5) unconformities between altered and unaltered rocks that indicate the episodic nature of magmatic and related hydrothermal events, (6) inferred depth of the underlying magma reservoir, and (7) models for fluxes of heat and magmatic fluids.

Hydrothermally-altered rocks on Mount Rainier are the product of (1) partly superimposed zones of alteration formed around the long-lived central magma conduit during and following periods of high magmatic fluid flux and (2) narrow zones of alteration around dikes mostly on the west and east flanks of the volcano (Figs. 5 and 11a). The distribution of eruptive rocks of different ages, erosional unconformities between these eruptive units, and an inferred tree-like cross-sectional distribution of hydrothermally-altered rock in permeable units in the core of the volcano indicate repeated cycles of edifice construction during periods of high magmatic eruption, overlapped and followed by hydrothermal alteration and erosion of the edifice during quiescent periods. Alteration was narrow around the central conduit system (≤1 km diameter), as visible in extensive headwall exposures of unaltered lava flows and breccias on the upper south, southwest, northwest, and north flanks of the volcano. Alteration extended much farther from the conduit system only on the upper west and east flanks of the edifice where concentrations of dikes provided heat and fluid during periods of high magma flux.

In the interior of the volcano, hydrothermal alteration assemblages likely were zoned along and around the central magma conduit. Alteration assemblages varied vertically with steam-heated and magmatic-steam assemblages near the surface, and deeper, higher temperature magmatic-hydrothermal assemblages in the core of the edifice (Fig. 11B), as inferred from altered clasts in the Osceola Mudflow and from the mineralogy of the F tephra. Lower intensity smectite–pyrite (argillic) alteration surrounded the shallow conduit system and extended into the west and east edifice flanks associated with dikes. Deeper parts of the smectite–pyrite association were transitional into interlayered illite/smectite and chlorite alteration (low-grade propylitic alteration), preserved now as clasts in the West Fork lobe of the Osceola Mudflow. The strong correlation between breccia textures and increased intensity of alteration is evidence that hydrothermal fluids were focused into permeable units, such as flow-top breccias and block-and-ash-flow deposits. Alteration likely followed beds that dip away from the summit much like sagging branches on a snow-covered tree. Water-saturated breccias near the summit of Mt. Adams are required to explain detailed geophysical data (Finn et al., 2007), supporting the concept that similar water-saturated layers existed within the pre-Osceola edifice at Mount Rainier. Within such breccias the reaction of aqueous fluids containing H_2S formed the generally weak smectite–pyrite alteration. Alunite and hypogene jarosite formed locally in shallow oxygenated zones where SO_2-rich magmatic gases vented. A relatively thin zone of steam-heated alteration underlay the summit but was removed by the collapse(s) that generated the Paradise lahar and the Main Fork lobe of the Osceola Mudflow. The deeper part of the steam-heated zone was comprised of smectite–pyrite alteration; this was transitional to the outer zone of magmatic-hydrothermal alteration,

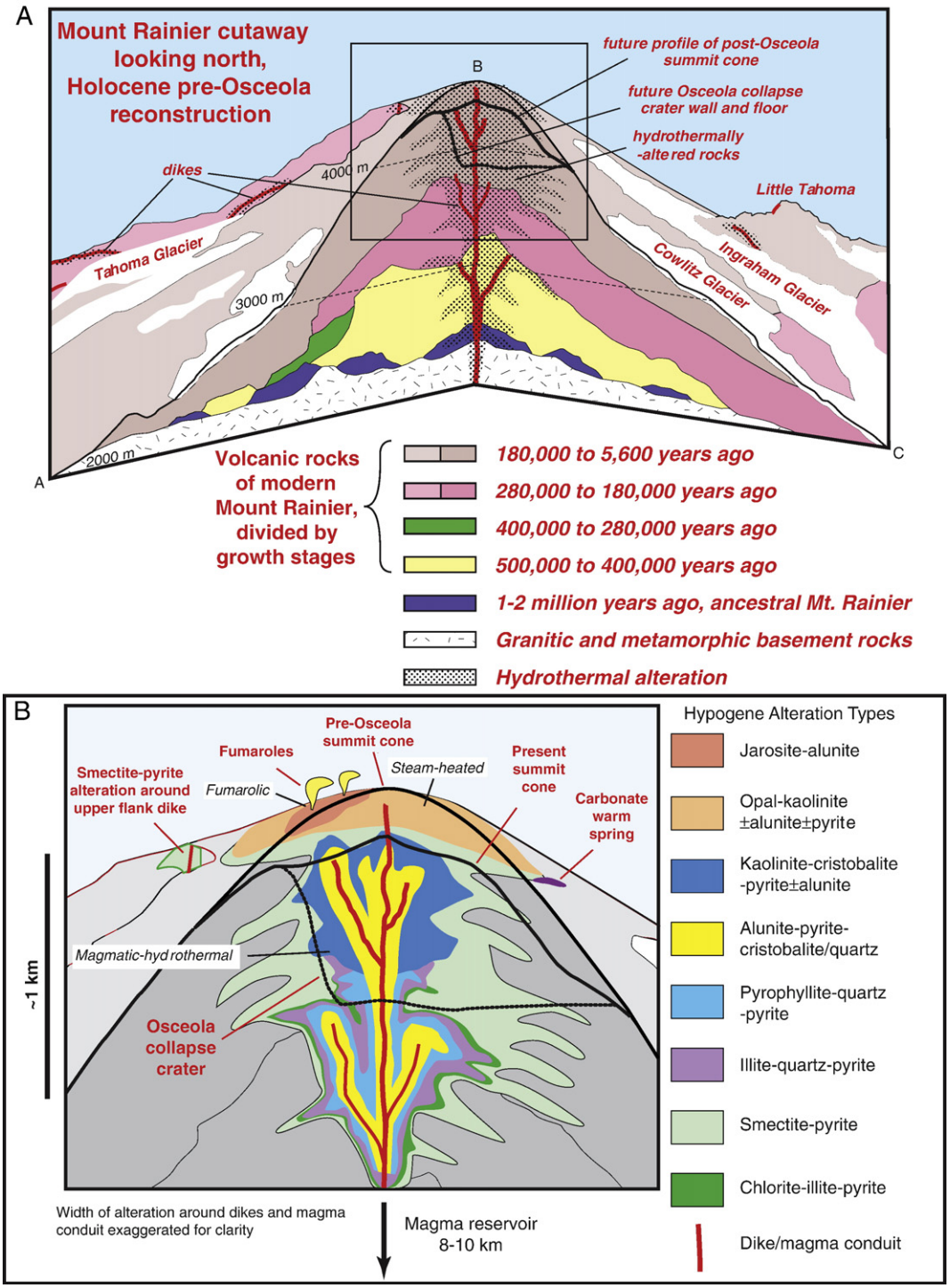

Fig. 11. Cutaway cross-sections of Mount Rainier showing models of the distribution of major eruptive units and hydrothermal alteration at 5600 y BP. (A) Entire edifice showing overall distribution of volcanic rocks. Box shows outline of area enlarged in b. (B) Inset of the upper part of Mount Rainier showing inferred distribution of hydrothermally-altered rocks and alteration assemblages prior to the Osceola Mudflow collapse, present-day hydrothermal alteration at summit, and hydrothermal environments. Upper part of pre-Osceola hydrothermal system was dominated by near-surface steam-heated and fumarolic alteration, with deeper, higher temperature magmatic-hydrothermal alteration zoned around the central magma conduit. Smectite–pyrite alteration formed in water-saturated, permeable breccia units at the base of the steam-heated alteration, in the outer fringes of magmatic-hydrothermal alteration, and in narrow zones around upper flank dikes. Osceola Mudflow and F tephra incorporated both shallow and deep alteration, whereas the Paradise lahar only sampled shallow alteration. Alteration was likely much narrower and less continuous than portrayed due to the deep magma reservoir (≥8–10 km) and restricted permeability. See text for additional description.

characterized in the edifice core by alunite, pyrophyllite, topaz, and pyrite with traces of enargite. Steam-heated, sulfate-rich fluids in the transition zone between magmatic-hydrothermal and steam-heated environments may have deposited anhydrite/gypsum. The phreato-magmatic nature of the F tephra eruptions, the presence of hydrothermally brecciated clasts in the Osceola Mudflow, and the formation of hypogene jarosite in fumaroles are evidence for a vigorous hydrothermal system in the edifice interior. Warm springs that deposited carbonate (dolomite), quartz, and pyrite, recorded by a single clast sample from the Osceola Mudflow, likely discharged along the margins of the hydrothermal system on the flanks of the edifice.

The similarity of altered clasts in the Osceola Mudflow to alteration assemblages in fossil hydrothermal systems, notably those related to high-sulfidation epithermal gold–silver deposits (e.g., Summitville, USA, Steven and Ratte, 1960, Stoffregen, 1987; Julcani, Peru, Deen et al., 1994), suggests similar zoning of magmatic-hydrothermal alteration around the central magma conduit at Mount Rainier (Fig. 11B). In these fossil hydrothermal systems, alteration is zoned outward over meters to tens of meters from a core of residual quartz, through quartz–alunite, quartz–pyrophyllite, dickite, or kaolinite, and quartz–illite assemblages, to distal quartz–smectite or chlorite assemblages (all containing abundant pyrite). This mineralogical zoning reflects both decreasing temperature and progressive neutralization of acid fluids by reaction with wall rocks (Steven and Ratte, 1960). At Mount Rainier, quartz–pyrophyllite assemblages and sulfur isotope fractionation indicate a maximum temperature of alteration, sampled by the Osceola Mudflow, of about 225–300 °C. Mineral associations and stable-isotope values indicate formation of this high-temperature alteration from acidic, sulfur-rich liquids with a large component of magmatic water (Fig. 9). Lower temperature assemblages indicate progressively smaller contributions of magmatic water. Despite the relatively deep (>8 km) magma storage inferred for Mount Rainier from melt inclusions, seismicity, and seismic velocities, and scarcity of peripheral vents and geothermal features, magmatic fluid flux was intermittently sufficient to reach the shallow edifice interior where volatile species condensed into ground water filling perched aquifers in permeable breccia units. The presence of quartz–topaz alteration and fluorite contained in high-temperature alteration assemblages sampled from the Osceola Mudflow and from the F tephra indicate fluxes of HF sufficient to stabilize these minerals. Topaz-bearing alteration assemblages also are present in Pleistocene magmatic-hydrothermal systems at Brokeoff and Maidu volcanoes near Lassen Peak (Fig. 1; John et al.,

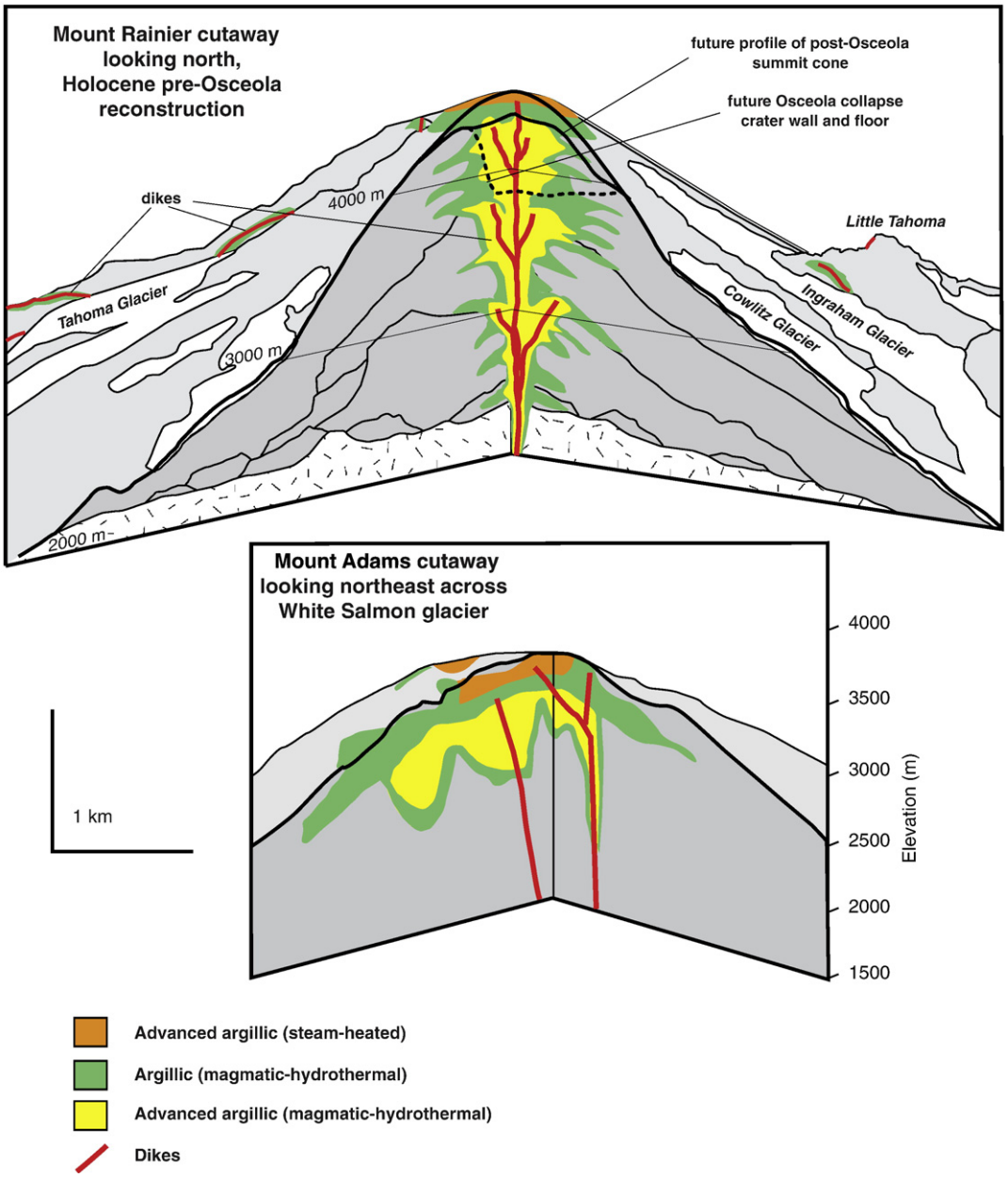

Fig. 12. Cutaway cross-sections of (A) Mount Rainier and (B) Mount Adams showing generalized distribution of hydrothermally-altered rock and inferred alteration environments and assemblages. Distribution of hydrothermally-altered rocks on Mount Rainier generalized from Fig. 11A showing inferred alteration prior to the Osceola Mudflow collapse at about 5600 y BP. Present-day distribution of hydrothermally-altered rocks on Mount Adams based on block model of the edifice from Finn et al. (2007, Fig. 10).

2005, 2006), suggesting that F-bearing alteration assemblages may be common in other hydrothermal systems in the Quaternary Cascades arc.

9.2. Implications for future edifice collapse at Mount Rainier

Large-volume, clay-rich debris flows younger than 5600 y BP originated on the west side of the edifice in Sunset Amphitheater (Crandell, 1971; Scott et al., 1995) (Figs. 4 and 7). Our analysis of clasts in these debris flows indicates that successively younger deposits contain increasingly complex alteration assemblages that resulted from higher temperature and more intense alteration conditions. This probably is due to progressive incision into remnants of the altered axial conduit system preserved in the back wall of the Osceola collapse crater. Unlike the summit, thermal features such as fumaroles are absent at Sunset Amphitheater. With the possible exception of a small and weak thermal anomaly detected remotely by infrared methods (Frank, 1985), the region undergoing collapse is hydrothermally inactive. Geophysical measurements image a substantial zone of strong alteration rooted in Sunset Amphitheater coincident with the western concentration of radial dikes on the upper edifice (Finn et al., 2001). Modeling of slope stability incorporating variable rock strengths due to hydrothermal alteration also identifies this area as most likely to fail (Reid et al., 2001). These findings suggest that future edifice collapse and large-volume, clay-rich debris flows will most likely originate from the upper west side of the volcano near Sunset Amphitheater.

9.3. Comparisons with Mount Adams and other Cascades stratovolcanoes

Some Cascades stratovolcanoes have appreciable hydrothermal alteration, whereas others do not. Significant upper-edifice alteration is exposed on Mounts Rainier and Adams, where multiple clay-rich debris flows have occurred in the Holocene; by contrast the edifice-eviscerating, debris-avalanche deposits from Mount St. Helens (1980) and Mount Shasta (Pleistocene; Crandell, 1989) are minimally altered. The presence or absence of Holocene glacial ice is unlikely to account for differences in the extent of alteration, because many of the Cascades stratovolcanoes grew mainly during the Pleistocene when ice was widespread at higher elevations throughout the range. A possible explanation for differences in alteration is eruptive style. Volcanoes that produce abundant interlayered lava flows and breccias, and perhaps vent facies breccias, create multiple permeable regions suitable for perched aquifers into which escaping magmatic volatiles can condense (Mounts Rainier, Adams, and Baker), in contrast to volcanoes that extrude dense lava domes and thick lava flows which are cut by through-going fractures that allow escape of magmatic volatiles to the atmosphere (Mounts St. Helens, Hood, Shasta, and Lassen Peak).

Hydrothermal alteration on Mount Adams (Finn et al., 2007) closely mirrors our interpretation of alteration on Mount Rainier shortly prior to the Osceola Mudflow collapse. We interpret the distribution of hydrothermally-altered rocks and alteration environments on sections through these volcanic edifices (Fig. 12). The upper part of the edifice at Mount Adams erupted in the past 10–40 kyr, with summit-forming andesite lava flows and interlayered breccias erupted at 10–15 kyr BP (Hildreth and Lanphere, 1994). Venting of H_2S from the summit crater and deposition of elemental sulfur beneath the summit ice cap indicates the presence of an active hydrothermal system. Models of the three-dimensional distribution of hydrothermal alteration on Mount Adams, based on detailed geophysical measurements, suggest a root of intensely altered rock filling a brecciated central magma conduit (Finn et al., 2007). Alteration at the top of Mount Adams comprises intense steam-heated advanced argillic assemblages (opal–kaolinite–alunite) and lateral and deeper argillic assemblages (mostly montmorillonite; Hildreth et al., 1983; Vallance 1999; Zimbelman et al., 2005; Finn et al., 2007). Outside an approximately 100-m-thick, blanket-like zone of steam-heated advanced argillic alteration, alteration is heterogeneously distributed; breccia matrices and small clasts are strongly altered, whereas interiors of larger clasts are unaltered. Only the steam-heated advanced argillic and argillic alteration assemblages

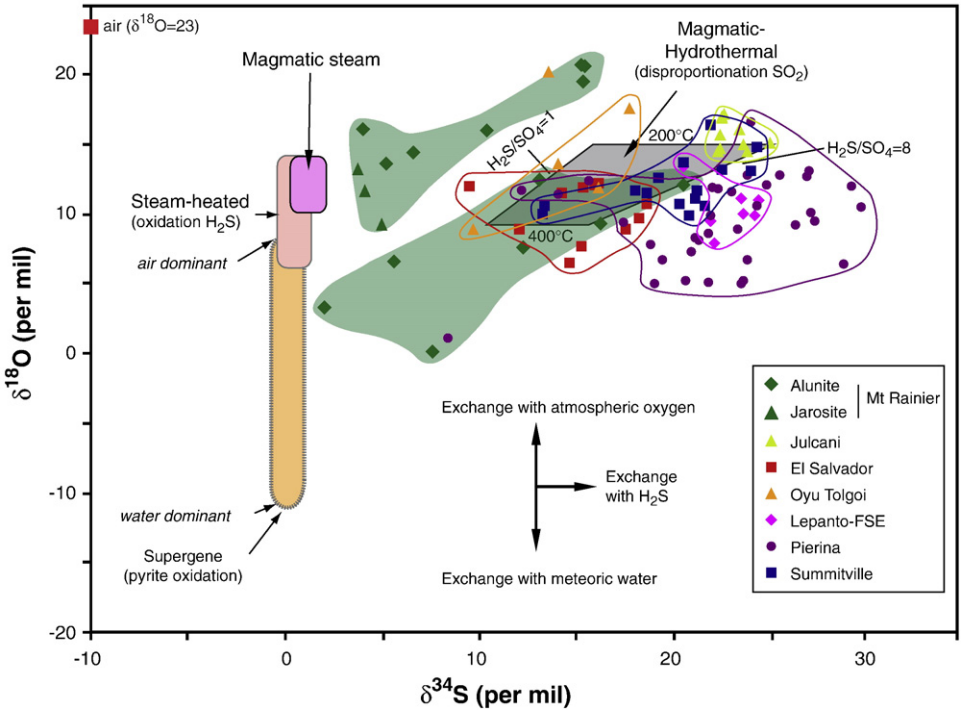

Fig. 13. Plot of S–O stable-isotope data for hypogene alunites and jarosites from Mount Rainier and hypogene alunites from porphyry copper and high-sulfidation epithermal gold–silver deposits. Reference fields are from Rye et al. (1992); see text and Fig. 8 for further details. Data sources: Mount Rainier, this study; Julcani, Peru—Deen et al. (1994); Lepanto—Far South East, Philippines—Hedenquist et al. (1998); El Salvador, Chile—Watanabe and Hedenquist (2001); Pierina, Peru—Fifarek and Rye (2005); Summitville, Colorado—Bethke et al. (2005); Oyu Tolgoi, Mongolia—Khasgerel et al. (2006).

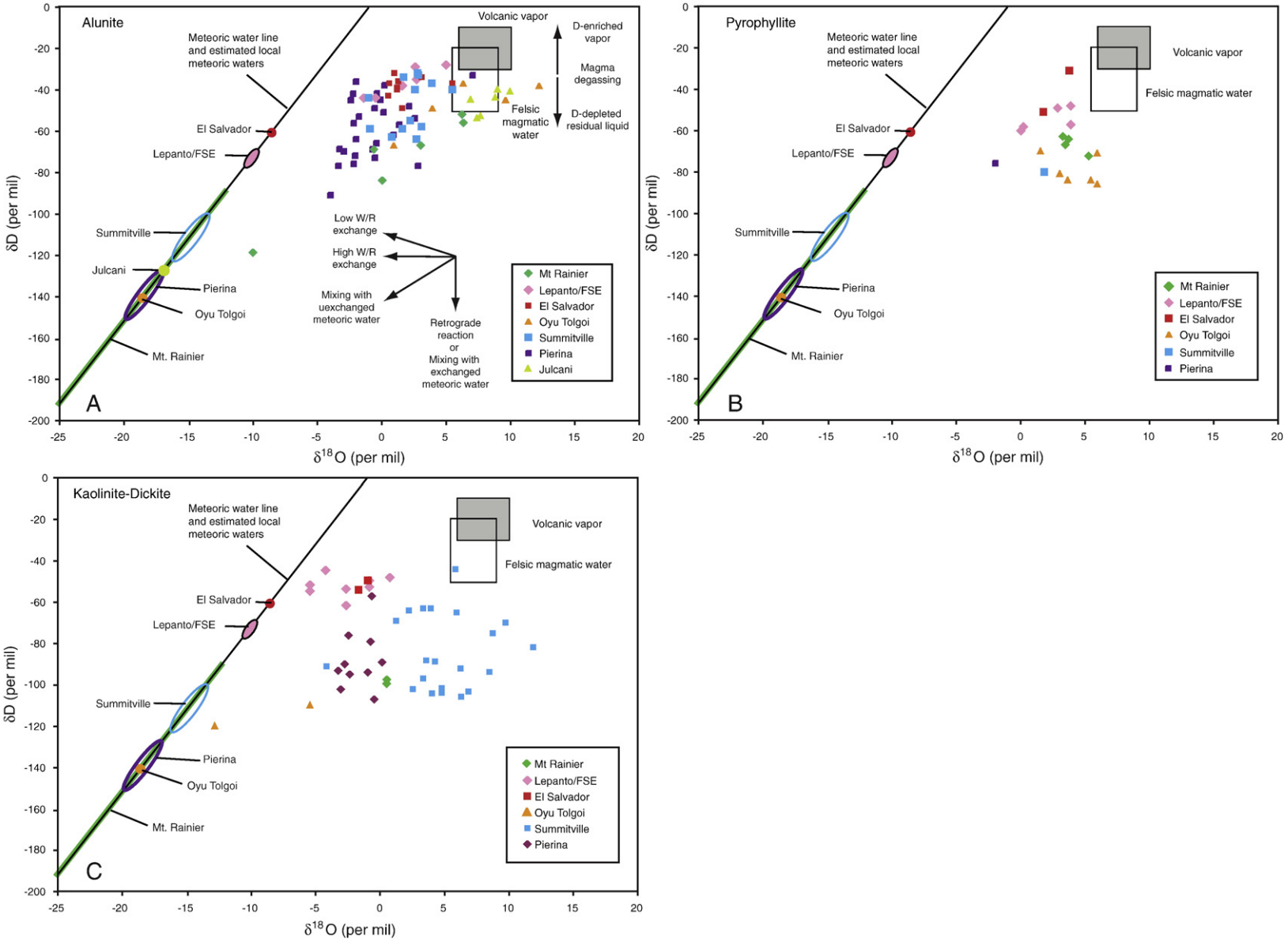

Fig. 14. Plot of δD and $\delta^{18}O$ values of calculated parent fluids for (A) alunites, (B) pyrophyllites, and (C) kaolinites from Mount Rainier compared with those from published studies of high-sulfidation epithermal gold–silver and porphyry copper deposits. All parent fluids recalculated using fractionation factors in Table 8. Arrows in A show expected mixing trends between magmatic fluids and unexchanged meteoric water, low temperature retrograde exchange with meteoric water, and the effects of exchange with wall rocks at high and low water/rock (W/R) ratios and of magma degassing on the deuterium contents of water in vapor and residual liquid phases (see Hedenquist et al., 1998; Bethke et al., 2005). These mixing and exchange trends apply to all three figures. Data sources: Mount Rainier, this study; Lepanto—Far South East, Philippines—Hedenquist et al. (1998); El Salvador, Chile—Watanabe and Hedenquist (2001); Oyu Tolgoi, Mongolia—Khasgerel et al. (2006); Summitville, Colorado—Bethke et al. (2005); Pierina, Peru—Fifarek and Rye (2005); Julcani, Peru—Deen et al. (1994).

from the upper parts of the hydrothermal system have been incised by Holocene debris flows on Mount Adams, although deeper advanced argillic magmatic-hydrothermal alteration assemblages present in the Osceola Mudflow and F tephra at Mount Rainier are likely present in the altered core of Mount Adams. The total volume of strongly altered rocks within the edifice of Mount Adams is estimated to be about 1.8 km^3 (Finn et al., 2007), similar to the volume of altered rock in the Osceola Mudflow.

9.4. Are porphyry copper or high-sulfidation epithermal deposits now forming beneath Mount Rainier?

Porphyry copper-(gold) and high-sulfidation epithermal gold–silver deposits can form at shallow depths beneath and around andesite–dacite stratovolcanoes in arcs along convergent plate margins (e.g., Sillitoe, 1973; Hedenquist and Lowenstern, 1994; Hattori and Keith, 2001; Sillitoe and Hedenquist, 2003; Halter et al., 2004). Numerous small porphyry copper deposits and high-sulfidation prospects are exposed in middle to late Tertiary rocks in Washington and Oregon, such as those that underlie Mount Rainier (Hollister, 1979; John et al., 2003). Although no porphyry copper deposits are known in the Quaternary Cascades arc, apparently unmineralized magmatic-hydrothermal alteration, of the type that is associated with high-sulfidation-style deposits, is present in eroded stratovolcanoes at the southern end of the arc near Lassen Peak (John et al., 2005, 2006).

Magmatic-hydrothermal alteration assemblages with residual quartz and sulfide-cemented hydrothermal breccias are present at Mount Rainier, as well as trace amounts of enargite, a Cu–As mineral characteristic of high-sulfidation epithermal deposits (Fig. 6H). However, several lines of evidence suggest that no significant high-sulfidation epithermal deposits are present and provide no indication that porphyry copper deposits are forming at shallow depths beneath or adjacent to Mount Rainier: (1) multiple periods of edifice construction and edifice degradation during the 500,000 years history of Quaternary Mount Rainier have not left evidence for shallowly emplaced plutons or domes; (2) spatially extensive areas of shallow alteration, such as zones of residual quartz, and alteration of older parts of the Quaternary edifice exposed beneath the present edifice are absent; (3) most alteration exposed on the volcano and typical of most clasts in the clay-rich debris flows is weak, quartz poor, and lacking quartz veins; (4) melt inclusions in Quaternary eruptive products indicate eruption from depths ≥4–10 km; and (5) seismic velocities and earthquake focal depths indicate an absence of a sizeable shallow (<8 km) magma reservoir (Moran et al., 1999, 2000).

The S and O isotope values for hypogene alunite and jarosite from Mount Rainier extend considerably beyond those observed for alunite in studies of high-sulfidation epithermal and porphyry mineral deposits (Fig. 13). Most of the isotopic values for the alunite in high-sulfidation ore deposits cluster near the magmatic-hydrothermal reference field. The range of $\delta^{34}S$ values for individual deposits reflects variations in the redox state and $\delta^{34}S_{\Sigma S}$ of the fluids, and the range of $\delta^{18}O$ values reflect the degree of interaction of meteoric water with magmatic-hydrothermal fluids (Rye et al., 1992). Some sulfate minerals on Mount Rainier have lower $\delta^{34}S$ values and much higher $\delta^{18}O_{SO_4}$ values than generally observed in ore deposits. These differences arise because alteration minerals that form in the shallowest environments near vents on the edifices of stratovolcanoes are seldom preserved in mineral deposits.

In contrast, the H and O isotope values of parent fluids of alunite, pyrophyllite, and kaolinite from Mount Rainier are within the range observed for these minerals from porphyry and high-sulfidation deposits (Fig. 14A,B,C) but their overall H and O isotope trend is less scattered (Fig. 9). The data for parent fluids for alunite (Fig. 14A) scatter around magmatic-ambient meteoric water mixing trends that can be defined for individual deposits. The variation of values around these trends in individual deposits can be explained by a combination of wall rock exchange, mixing, and deuterium depletion due to magma degassing (for summary, see Bethke et al., 2005, Fig. 14; Hedenquist et al., 1998, Fig. 18). Not all data for parent fluids of pyrophyllite and kaolinite in individual deposits are readily explained by simple magmatic-meteoric water mixing, such as seen for the Mt. Rainier samples (Fig. 9). There is a suggestion in the data for these minerals (Figs. 14B and c) that specific patterns of H and O values for pyrophyllite and kaolinite from individual deposits depend on the isotope composition of local meteoric water and that the lower the δD value of the ambient meteoric water, the greater the tendency for δD values of parent fluids to fall off of a simple mixing trend. While low δD values for some of the kaolinite and pyrophyllite may reflect deuterium depletion of residual fluids during magmatic degassing with subsequent meteoric water mixing (Taylor, 1992; Hedenquist et al., 1998), some low values most likely reflect retrograde hydrogen exchange with meteoric water without accompanying oxygen isotopic exchange typical for phyllosilicates (O'Neil and Kharaka, 1976). Perhaps, the scatter of δD values in hydrous minerals is more evident in ore deposits than on Mount Rainier, because ore deposition is a product of sustained hydrothermal systems with pronounced waxing and waning phases which would allow for much greater variation in δD of hydrous minerals. Thus, the stable-isotope data are consistent with the absence of shallow high-level intrusions at Mount Rainier that could support the large, long-lived hydrothermal systems that are a requirement to form high-sulfidation and porphyry-type ore deposits.

10. Conclusions

Mount Rainier grew episodically over the past 500,000 years with alternating protracted periods of high and low rates of magma eruption. Alteration by hydrothermal fluids was particularly intense and focused into permeable breccia units during and immediately following times of high eruption rates. This alteration promoted edifice degradation during ensuing times of relative volcanic quiescence. Hydrothermal–mineral assemblages and distributions at Mount Rainier can be understood in the framework of hydrothermal processes and environments developed from studies of ore deposits. Mineral assemblages and stable-isotope compositions of hydrothermally-altered rocks in outcrop, in clasts in Holocene debris flows, and in the F tephra indicate that alteration formed from variable mixtures of magmatic and meteoric water at temperatures from <100 °C to ~300 °C. Diversity in mineral assemblages and intensity of alteration were controlled by position in the edifice, by permeability, and by variations in the size of the hydrothermal system linked to the flux of magmatic heat and volatiles. High-temperature magmatic-hydrothermal and overlying surficial steam-heated and fumarolic alteration assemblages were limited to the central conduit system and near-summit part of the volcano that was affected by hot magmatic fluids. Intense pyrite-rich alunite- and pyrophyllite-bearing alteration assemblages formed in the interior of the edifice during episodes dominated by magmatic water fluids. In contrast, generally weak, low-temperature smectite ±pyrite alteration developed surrounding this core zone, but within ~1 km from the edifice axis, and extended to the upper east and west flanks of the volcano only during periods of high magmatic flux accompanied by dike emplacement. Hydrothermal fluids that caused edifice flank alteration were greatly diluted and cooled by meteoric water. Strong alteration on the edifice flanks was limited to narrow (≤5 m) zones bordering dikes, whereas surrounding, more diffuse, flank alteration was caused by outflow of hydrothermal fluids during times of heightened magmatic activity. Though visually apparent, this diffuse alteration is weak and of little significance for edifice stability. Alteration in both the central core and lower flanks was controlled by permeability. The most strongly altered rocks are breccias, and adjacent, more massive rocks are weakly altered or unaltered. Permeable flow-top breccias, lava talus deposits, and block-and-

ash-flow deposits high on the edifice were locally meteoric-water-saturated and acted as perched aquifers that focused alteration along beds that dipped radially away from the central magma conduit. Volcanoes such as Mounts Rainier and Adams with abundant near-conduit upper-edifice breccias are prone to alteration, whereas volcanoes that are breccia-poor (e.g. massive domes) are not.

Intensely altered rocks from the summit, east flank, and edifice interior of Mount Rainier were removed by the Osceola Mudflow collapse. The most intense in-situ alteration remaining is exposed in Sunset Amphitheater on the uppermost west flank of the volcano. Successively younger debris-flow deposits originating from this area have revealed progressively more strongly altered rocks with higher temperature alteration assemblages. The most recent debris flow (early 20th century Tahoma Glacier rockfall) contains alteration assemblages only observed elsewhere in the Osceola Mudflow and F tephra suggesting that the headwall exposures are approaching the core of an older hydrothermal system. Geophysical studies also identify this area to be underlain by the most extensive subsurface alteration (Finn et al., 2001), and altered rocks from this area have the potential to produce a large clay-rich debris flow.

Although hydrothermal–mineral assemblages and stable-isotope compositions of altered rocks are similar to those found in high-sulfidation epithermal gold–silver deposits and in altered rocks overlying porphyry copper deposits, the typical deep location of past (≥4–10 km) and present (>8 km) magma reservoirs, the absence of exposed altered shallow Quaternary intrusions and domes, and the relatively sparse occurrences of alteration assemblages typical of these deposits in the debris flows that effectively expose the stratovolcano to depths of up to 1–1.5 km are not encouraging indicators for deeper mineral deposits at Mount Rainier.

Acknowledgements

We thank the National Park Service for permission to work within Mount Rainier National Park and collect samples. Geoff Plumlee and Ed du Bray helped with field work. Rhonda Driscoll and Kathryn Flynn prepared samples for mineralogic and XRD studies. Cynthia Kester, Cayce Gulbransen, William Christiansen, and Pamela Gemery performed stable-isotope analyses, and Cyrus Berry made many of the sulfur speciation analyses. Phil Bethke, Jake Lowenstern, Jeremy Richards, and Jeff Hedenquist are thanked for helpful reviews of earlier versions of this manuscript.

Appendix A. Analytical methods

Approximately 325 variably altered rock, lahar matrix (−10 mesh fraction), and tephra samples were collected from Quaternary units on and near Mount Rainier (Fig. 5 and Supplementary data). The constituent minerals were identified using a combination of optical microscopy, powder X-ray diffraction (XRD), scanning electron microscopy (SEM), and shortwave infrared spectroscopy. Polished thin sections of about 80 altered rocks were examined in transmitted and reflected light. XRD was applied to ground bulk samples and hand-picked grains using CuKα radiation from 4° to 64° 2Ø with step size of 0.02° and a count time of 2 s/step. Clay-sized separates (<1 μm) from 30 rock and lahar matrices were separated by centrifugation. Oriented mounts prepared from the <1 μm separates were scanned using CuKα radiation from 2 to 40° 2Ø as air-dried, saturated with ethylene glycol, heated to 375 °C, and heated to 550 °C. About 40 thin sections, 20 rock chips and 5 grain mounts were examined in back-scatter and secondary electron modes using an SEM equipped with an energy dispersive analyzer. Most altered rocks were scanned using a Portable Infrared Mineral Analyzer (PIMA), which allows identification of hydrous phases (e.g., clay minerals, pyrophyllite, micas, and chlorite), sulfates (alunite, jarosite, gypsum), carbonates, and topaz (Thompson et al., 1999).

Whole-rock chemical analyses of about 40 samples of altered clasts in debris flows, lahar matrices, and altered outcrops are summarized in Table 3. Samples were dissolved using a hydrochloric, nitric, perchloric, and hydrofluoric acid digestion and analyzed for 42 elements using ICP-MS and ICP-AES methods. In addition, gold was analyzed by fire assay and mercury by cold vapor atomic absorption techniques. Total sulfur contents of 80 lahar matrix, glacial till, and tephra samples were measured by combustion (Brown and Curry, 2002). Tests of the analytical methods determined accuracy within 20 relative percent for all measured parameters. Uncertainty increased within 5 times the lower-limit of detection.

Sulfur-bearing phases were sequentially extracted using chemical reagents to estimate phase abundance and to recover sulfur and sulfate for isotopic analysis (Berry and Breit, 2007). Chemical extraction was required, because the sulfur-bearing phases were generally fine grained (<100 μm) and sufficiently intergrown such that mechanical separation was impractical. The extraction procedure separately recovers elemental sulfur, water-soluble sulfates (anhydrite/gypsum), jarosite, pyrite, and alunite/barite. Replicate extraction analyses were within 10 relative percent for each phase measured. All phases were analyzed to determine their $\delta^{34}S$ composition, and the anhydrite/gypsum, jarosite, and alunite/barite fractions were analyzed to determine $\delta^{18}O$. Purified mineral separates using standard physical separation techniques were used for isotopic analysis of minerals in some clasts and tephras. Oxygen and hydrogen isotopes were analyzed for clay-sized separates from 10 altered clasts, as well as for 6 alunite separates.

Most sulfur isotope analyses were made by continuous flow mass spectrometry similar to that described by Giesemann et al. (1994) using an elemental analyzer on an Optima MicroMass mass spectrometer. Hydrogen isotope analyses of hydrous minerals and oxygen isotope analyses of sulfates were made by continuous flow techniques through a TC/EA coupled to a ThermoFinnigan Delta XL mass spectrometer using techniques similar to those described by Sharp et al. (2001). Oxygen isotope analyses of hydrous minerals were made on CO_2 prepared by the BrF_5 technique of Clayton and Mayeda (1963) followed by conventional analyses on a Finnigan MAT 252 mass spectrometer. Precision is ±0.2‰ for sulfur isotope data; ±2‰ for hydrogen; ±0.5‰ for $\delta^{18}O$ of sulfates and ±0.2 for hydrous minerals. Results of the isotopic analyses are listed in Tables 6 and 7.

Appendix B. Supplementary data

Supplementary data associated with this article can be found, in the online version, at doi:10.1016/j.jvolgeores.2008.04.004.

References

Arribas Jr., A., 1995. Characteristics of high-sulfidation epithermal deposits, and their relation to magmatic fluid. In: Thompson, J.F.H. (Ed.), Magmas, Fluids, and Ore Deposits. Mineral. Assoc. Canada Short Course Series, vol. 23, pp. 419–454.

Berry, C.J., Breit, G.N., 2007. Sequential extraction of sulfur-containing minerals from hydrothermally altered volcanic rocks for stable isotope analysis [ab.]. Geol. Soc. Am. Abstr. with Prog. 39, 464.

Bethke, P.M., Rye, R.O., Stoffregen, R.E., Vikre, P., 2005. Evolution of the magmatic-hydrothermal acid–sulfate system at Summitville, Colorado: integration of geological, stable-isotope, and fluid inclusion evidences. Chem. Geol. 215, 281–315.

Brown, Z.A., Curry, K.J., 2002. Total sulfur by combustion. In: Taggert, J.E. (Ed.), Analytical Methods for Chemical Analysis of Geologic and Other Materials. U.S. Geol. Surv. Open-File Report 02-223, pp. Q1–Q4.

Bruce, V.L., 1998. Geochemistry of hydrothermal alteration along a radial transect from the summit of Mount Rainier, Washington. MS thesis, Univ. California, Riverside.

Clayton, R.N., Mayeda, T.K., 1963. The use of bromine pentafluoride in the extraction of oxygen from oxides and silicates for isotopic analysis. Geochim. Cosmochim. Acta. 27, 43–52.

Cole, D.R., Ripley, E.M., 1999. Oxygen isotope fractionation between chlorite and water from 170 ° to 350 °C: a preliminary assessment based on partial exchange and fluid/rock experiments. Geochim. Cosmochim. Acta. 63, 449–457.

Crandell, D.R., 1971. Postglacial lahars from Mount Rainier volcano, Washington. U.S. Geol. Surv. Prof. Pap. 677. 75 p.

Crandell, D.R., 1989. Gigantic debris avalanche of Pleistocene age from ancestral Mount Shasta volcano, California, and debris-avalanche hazard zonation. U.S. Geol. Surv. Bull. 1861. 32 pp.

Crandell, D.R., Waldron, H.H., 1956. A recent volcanic mudflow of exceptional dimensions from Mt. Rainier, Washington. Am. J. Sci. 254, 349–362.
Craig, H., 1961. Isotopic variations in meteoric water. Science. 133, 1702–1703.
Crowley, J.K., Zimbelman, D.R., 1997. Mapping hydrothermally altered rocks on Mount Rainier, Washington, with airborne visible/infrared imaging spectrometer (AVIRIS) data. Geology 25, 559–562.
Deen, J.A., Rye, R.O., Munoz, J.L., Drexler, J.W., 1994. The magmatic-hydrothermal system at Julcani, Peru; evidence from fluid inclusions and hydrogen and oxygen isotopes. Econ. Geol. 89, 1924–1938.
Fifarek, R.H., Rye, R.O., 2005. Stable isotope geochemistry of the Pierina high-sulfidation Au–Ag deposit, Peru: influence of hydrodynamics on SO_4^{2-}–H_2S sulfur isotope exchange in magmatic-steam and steam-heated environments. Chem. Geol. 215, 253–279.
Finn, C.A., Sisson, T.W., Deszcz-Pan, M., 2001. Aerogeophysical measurements of collapse-prone hydrothermally altered zones at Mount Rainier volcano. Nature 409, 600–603.
Finn, C.A., Deszcz-Pan, M., Anderson, E.A., John, D.A., 2007. Three dimensional geophysical mapping of rock alteration and water content at Mount Adams, Washington: implications for lahar hazards. J. Geophys. Res. 112, B10204.
Fiske, R.S., Hopson, C.A., Waters, A.C., 1963. Geology of Mount Rainier National Park, Washington. U.S. Geol. Surv. Prof. Pap. 444. 93 pp.
Frank, D.G., 1985, Hydrothermal processes at Mount Rainier, Washington. Ph.D. Thesis, Univ. Washington, Seattle.
Frank, David, 1995. Surficial extent and conceptual model of hydrothermal system at Mount Rainier, Washington. J. Volcanol. Geotherm. Res. 65, 51–80.
Giesemann, A., Jager, H.J., Norman, A.L., Krouse, H.R., Brand, W.A., 1994. On-line sulphur-isotope determination using an elemental analyzer coupled to a mass spectrometer. Anal. Chem. 66, 2816–2819.
Giggenbach, W.F., 1992. Isotopic shifts in waters from geothermal and volcanic systems along convergent plate boundaries and their origin. Earth Planet. Sci. Letters 113, 495–510.
Giggenbach, W.F., 1997. The origin and evolution of fluids in magmatic-hydrothermal systems, In: Barnes, H.L. (Ed.), Geochemistry of Hydrothermal Ore Deposits, 3rd Ed. John Wiley and Sons, Inc., New York, pp. 737–796.
Graham, C.M., Atkinson, J., Harmon, R.S., 1984. Hydrogen isotope fractionation in the system chlorite-water. Prog. Exp. Petrol. 6, 139–140.
Halter, W.E., Bain, N., Becker, K., Heinrich, C.A., Landtwing, M., Von Quadt, A., Bissig, T., Clark, A.H., Sasso, A.M., Tosdal, R.M., 2004. From andesitic volcanism to the formation of a porphyry–Cu–Au mineralizing magma chamber: the Farallón Negro Volcanic Complex, northwestern Argentina. J. Volcanol. Geotherm. Res. 136, 1–30.
Hattori, K.H., Keith, J.D., 2001. Contribution of mafic melt to porphyry copper mineralization: evidence from Mount Pinatubo, Philippines, and Bingham Canyon, Utah, USA. Mineralium Deposita. 36, 799–806.
Hedenquist, J.W., Lowenstern, J.B., 1994. The role of magmas in the formation of hydrothermal ore deposits. Nature 370, 519–527.
Hedenquist, J.W., Arribas Jr., A., Reynolds, T.J., 1998. Evolution of an intrusion-centered hydrothermal system: Far Southeast–Lepanto porphyry and epithermal Cu–Au deposits, Philippines. Econ. Geol. 93, 373–404.
Hedenquist, J.W., Arribas Jr., A., Gonzalez-Urien, E., 2000. Exploration for epithermal gold deposits. In: Hagemann, S.G., Brown, P.E. (Eds.), Gold in 2000. Rev. Econ. Geol., vol. 13, pp. 245–277.
Hemley, J.J., Montoya, J.W., Marinenko, J.W., Luce, R.W., 1980. Equilibria in the system Al_2O_3–SiO_2–H_2O and some general implications for alteration/mineralization processes. Econ. Geol. 75, 210–228.
Henley, R.W., Ellis, A.J., 1983. Geothermal systems ancient and modern: a geochemical review. Earth Sci. Rev. 19, 1–50.
Hildreth, W., 2007. Quaternary magmatism in the Cascades—geologic perspectives. U.S. Geol. Surv. Prof. Pap. 1744 125 pp. http://pubs.usgs.gov/pp/pp1744/.
Hildreth, W., Lanphere, M.A., 1994. Potassium–argon geochronology of a basalt–andesite–dacite arc system; the Mount Adams volcanic field, Cascade Range of southern Washington. Geol. Soc. Am. Bull. 106, 1413–1429.
Hildreth, W., Fierstein, J.E., Miller, M.S., 1983. Mineral and geothermal resource potential of the Mount Adams Wilderness and contiguous roadless area, Skamania and Yakima counties, Washington. U.S. Geol. Surv. Open-File Report 83-0474. 35 pp.
Hoblitt, R.P., Walder, J.S., Driedger, C.L., Scott, K.M., Pringle, P.T., Vallance, J.W., 1998. Volcano hazards from Mount Rainier, Washington, rev. 1998. U.S. Geol. Surv. Open-File Report 98-428. 11 p.
Hollister, V.F., 1979. Porphyry copper-type deposits of the Cascade volcanic arc, Washington. Minerals Sci. Eng. 11, 22–34.
John, D.A., Rytuba, J.J., Ashley, R.P., Blakely, R.J., Vallance, J.W., Newport, G.R., Heinemeyer, G.R., 2003. Field guide to hydrothermal alteration in the White River altered area and in the Osceola Mudflow, Washington. U.S. Geol. Surv. Bull. 2217 48 pp., http://geopubs.wr.usgs.gov/bulletin/b2217.
John, D.A., Rytuba, J.J., Breit, G.N., Clynne, M.A., Muffler, L.J.P., 2005. Hydrothermal alteration in Maidu Volcano: a shallow fossil acid–sulfate magmatic-hydrothermal system in the Lassen Peak area, California. In: Rhoden, H.N., Steininger, R.C., Vikre, P.G. (Eds.), Symposium 2005: Window to the World, Geol. Soc. Nevada, Reno, pp. 295–313.
John, D.A., Breit, G.N., Lee, R.G., Dilles, J.H., Muffler, L.J.P., Clynne, M.A., 2006. Fossil magmatic-hydrothermal systems in Pleistocene Brokeoff Volcano, Lassen Volcanic National Park, California [abs.]. EOS, vol. V53A–1745.
Khasgerel, B.-E., Rye, R.O., Hedenquist, J.W., Kavalieris, Imants, 2006. Geology and reconnaissance stable isotope study of the Oyu Tolgoi porphyry Cu–Au system, south Gobi, Mongolia. Econ. Geol. 101, 503–522.
Kirn, S.L., 1995. Petrology of a Mount Rainier pyroclastic eruption. B.Sc. thesis, Brown Univ., Providence, Rhode Island, USA.
Lescinsky, D.T., Sisson, T.W., 1998. Ridge-forming, ice-bounded lava flows at Mount Rainier, Washington. Geology 26, 351–354.
Luhr, J., Carmichael, I.S.E., Varekamp, J., 1984. The 1982 eruption of El Chichon Volcano, Chiapas, Mexico: mineralogy and petrology of the anhydrite-bearing pumices. J. Volcanol. Geotherm. Res. 23, 69–108.
Marumo, K., Nagasawa, K., Kuroda, Y., 1980. Mineralogy and hydrogen isotope geochemistry of clay minerals in the Ohnuma geothermal area, northeastern Japan. Earth Planet. Sci. Let. 47, 255–262.
Mattinson, J.M., 1977. Emplacement history of the Tatoosh volcanic–plutonic complex, Washington: ages of zircons. Geol. Soc. Am. Bull. 88, 1509–1514.
McKenna, J.M., 1994, Geochemistry and petrology of Mount Rainier magmas: Petrogenesis at an arc-related stratovolcano with multiple vents. M.Sc. thesis, Univ. Washington, Seattle.
Meyer, C., Hemley, J.J., 1967. Wall rock alteration. In: Barnes, H.L. (Ed.), Geochemistry of Hydrothermal Ore Deposits. Holt, Rinehart, and Winston, Inc., New York, pp. 166–235.
Moran, S.C., Lees, J.M., Malone, S.D., 1999. P wave velocity structure in the greater Mount Rainier area from local earthquake tomography. J Geophys. Res. 104, 10775–10786.
Moran, S.C., Zimbelman, D.R., Malone, S.D., 2000. A model for the magmatic-hydrothermal system at Mount Rainier, Washington, from seismic and geochemical observations. Bull. Volcanol. 61, 425–436.
Mullineaux, D.R., 1974. Pumice and other pyroclastic deposits in Mount Rainier National Park, Washington. U.S. Geol. Surv. Bull. 1326. 83 pp.
Ohmoto, H., Rye, R.O., 1979. Isotopes of sulfur and carbon, In: Barnes, H.L. (Ed.), Geochemistry of Hydrothermal Ore Deposits, 2nd Ed. Wiley-Interscience, New York, pp. 509–567.
O'Neil, J.R., Kharaka, Y.K., 1976. Hydrogen and oxygen isotope exchange reactions between clay minerals and water. Geochim. Cosmochim. Acta. 40, 241–246.
Reid, M.E., Sisson, T.W., Brien, D.L., 2001. Volcano collapse promoted by hydrothermal alteration and edifice shape, Mount Rainier, Washington. Geology 29, 779–782.
Reiners, P.W., Ehlers, T.A., Garver, J.I., Mitchell, S.G., Montgomery, D.R., Vance, J.A., Nicolescu, S., 2002. Late Miocene exhumation and uplift of the Washington Cascade Range. Geology 30, 767–770.
Reyes, A.G., 1990. Petrology of Philippine geothermal systems and the application of alteration mineralogy to their assessment. J. Volcanol. Geotherm. Res. 43, 279–309.
Rye, R.O., 1993. The evolution of magmatic fluids in the epithermal environment: the stable isotope perspective. Econ. Geol. 88, 733–753.
Rye, R.O., 2005. A review of the stable isotope geochemistry of sulfate minerals in selected igneous environments and related hydrothermal systems. Chem. Geol. 215, 5–36.
Rye, R.O., Bethke, P.M., Wasserman, M.D., 1992. The stable isotope geochemistry of acid–sulfate alteration. Econ. Geol. 87, 225–262.
Rye, R.O., Breit, G.N., Zimbelman, D.R., 2003. Preliminary mineralogic and stable isotope studies of altered summit and flank rocks and Osceola Mudflow deposits on Mount Rainier, Washington. U.S. Geol. Surv. Open-File Report 03-464. 26 pp.
Savin, S.M., Lee, M., 1988. Isotope studies of phyllosilicates. Rev. Mineral. 19, 189–219.
Schoen, R., White, D.E., Hemley, J.J., 1974. Argillization by descending acid at Steamboat Springs, Nevada. Clays Clay Miner. 22, 1–22.
Scott, K.M., Vallance, J.W., Pringle, P.T., 1995. Sedimentology, behavior, and hazards of debris flows at Mount Rainier, Washington. U.S. Geol. Surv. Prof. Pap. 1547. 56 p.
Sharp, Z.D., Atudorei, Durakiewicz, 2001. A rapid method for determination of hydrogen an oxygen isotope ratios from water and hydrous minerals. Chem. Geol. 178, 197–210.
Sheppard, S.M.F., Gilg, H.A., 1996. Stable isotope geochemistry of clay minerals. Clay Miner. 31, 1–24.
Sillitoe, R.H., 1973. The tops and bottoms of porphyry copper deposits. Econ. Geol. 68, 799–815.
Sillitoe, R.H., Hedenquist, J.W., 2003. Linkages between volcanotectonic settings, ore fluid compositions, and epithermal precious metal deposit. In: Simmons, S.G., Graham, Ian (Eds.), Volcanic, Geothermal, and Ore-forming Fluids: Rulers and Witnesses of Processes within the Earth. Soc. Econ. Geol. Spec. Pub., vol. 10, pp. 315–343.
Simmons, S.F., White, N.C., John, D.A., 2005. Geological characteristics of epithermal precious and base metal deposits. In: Hedenquist, J.W., Thompson, J.F.H., Goldfarb, R.J., Richards, J.P. (Eds.), Econ. Geol. One Hundredth Anniversary Volume, pp. 485–522.
Sisson, T.W., Lanphere, M.A., 1997. The growth of Mount Rainier volcano, Cascade arc, USA: Puerto Vallarta Mexico. International Association of Volcanology and Chemistry of the Earth's Interior General Assembly, p. 5.
Sisson, T.W., Vallance, J.W., Pringle, P.T., 2001. Progress made in understanding Mount Rainier's hazards. EOS 82 (9), 113–120.
Steven, T.A., Ratte, J.C., 1960. Geology of ore deposits of the Summitville district, San Juan Mountains, Colorado. U.S. Geol. Surv. Prof. Pap. 343. 70 p.
Stockstill, K.R., Vogel, T.A., Sisson, T.W., 2002. Origin and emplacement of the andesite of Burroughs Mountain, a zoned, large-volume lava flow at Mount Rainier, Washington, USA. J. Volcanol. Geotherm. Res. 119, 275–296.
Stoffregen, R.E., 1987. Genesis of acid–sulfate alteration and Au-Cu-Ag mineralization at Summitville, Colorado. Econ. Geol. 82, 1575–1591.
Stoffregen, R.E., Rye, R.O., Wasserman, D.M., 1994. Experimental studies of alunite I: ^{18}O–^{16}O and D–H fractionation factors between alunite and water at 250 °–450 °C. Geochim. Cosmochim. Acta. 58, 903–916.
Symonds, R.B., Janik, C.J., Evans, W.C., Ritchie, B.E., Counce, D., Poreda, R.J., Iven, M., 2003a. Scrubbing masks magmatic degassing during repose at Cascade-Range and Aleutian-Arc volcanoes. U.S. Geol. Surv. Open File Report 03-435. 22 pp.
Symonds, R.B., Poreda, R.J., Evans, W.C., Janik, C.J., Ritchie, B.E., 2003b. Mantle and crustal sources of carbon, nitrogen, and noble gases in Cascade-Range and Aleutian-Arc volcanic gases. U.S. Geol. Surv. Open File Report 03-436. 26 pp.
Taylor, B.E., 1992. Degassing of H_2O from rhyolitic magma during eruption and shallow intrusion, and the isotopic composition of magmatic water in hydrothermal systems. Geol. Surv. Japan Report 279, 190–194.
Taylor, B.E., Wheeler, M.C., Nordstrom, D.K., 1984. Stable isotope geochemistry of acid mine drainage: experimental oxidation of pyrite. Geochim. Cosmochim. Acta 48, 2669–2678.

Thompson, A.J.B., Hauff, P.L., Robitaille, A.J., 1999. Alteration mapping in exploration: application of short-wave infrared (SWIR) spectroscopy. Soc. Econ. Geol. Newslett. 39 13 pp.
Vallance, J.W., 1999. Postglacial lahars and potential hazards in the White Salmon River system on the southwest flank of Mount Adams, Washington. U. S. Geol. Surv. Bull. 2161 49 pp.
Vallance, J.W., Scott, K.M., 1997. The Osceola Mudflow from Mount Rainier: sedimentology and hazards implications of a huge clay-rich lahar. Geol. Soc. Am. Bull. 109, 143–163.
Vance, J.A., Clayton, G.A., Mattinson, J.M., Naeser, C.W., 1987. Early and middle Cenozoic stratigraphy of the Mount Rainier–Tieton River area, southern Washington Cascades. Washington Div. Geol. Earth Res. Bull. 77, 269–290.
Venezky, D., Rutherford, M.J., 1997. Pre-eruption conditions and timing of dacite–andesite mixing in the 2.2 ka C-layer at Mount Rainier. J. Geophys. Res., 102, 20069–20086.
Walsh, T.J., Korosec, M.A., Phillips, W.M., Logan, R.L., Schasse, H.W., 1987, Geologic map of Washington—Southwest quadrant: Washington Department of Natural Resources, Division of Geology and Earth Resources Geologic Map GM-34, scale 1:250,000.
Watanabe, Y., Hedenquist, J.W., 2001. Mineralogical and stable isotope zonation at the surface over the El Salvador porphyry copper deposit, Chile. Econ. Geol. 96, 1775–1797.
Wells, R.E., Weaver, C.S., Blakely, R.J., 1998. Fore-arc migration in Cascadia and its neotectonic significance. Geology 26, 759–762.
Zimbelman, D.R., 1996, Hydrothermal alteration and its influence on volcanic hazards Mount Rainier, Washington, a case history: PhD Thesis, Univ. Colorado, Boulder.
Zimbelman, D.R., Rye, R.O., Landis, G.P., 2000. Fumaroles in ice caves on the summit of Mount Rainier—preliminary stable isotope, gas, and geochemical studies. J. Volcanol. Geotherm. Res. 97, 457–473.
Zimbelman, D.R., Rye, R.O., Breit, G.N., 2005. Origin of secondary sulfate minerals on active andesitic stratovolcanoes. Chem. Geol. 215, 37–60.